INFECTIOUS DISEASES

Neutrophil extracellular traps drive inflammatory pathogenesis in malaria

Sebastian Lorenz Knackstedt[1], Athina Georgiadou[2], Falko Apel[1], Ulrike Abu-Abed[3], Christopher A. Moxon[4,5], Aubrey J. Cunnington[2], Bärbel Raupach[1], Deirdre Cunningham[6], Jean Langhorne[6], Renate Krüger[7], Valentina Barrera[8], Simon P. Harding[8], Aase Berg[9], Sam Patel[10], Kari Otterdal[11], Benjamin Mordmüller[12,13], Evelin Schwarzer[14], Volker Brinkmann[3], Arturo Zychlinsky[1], Borko Amulic[1,15]*

Neutrophils are essential innate immune cells that extrude chromatin in the form of neutrophil extracellular traps (NETs) when they die. This form of cell death has potent immunostimulatory activity. We show that heme-induced NETs are essential for malaria pathogenesis. Using patient samples and a mouse model, we define two mechanisms of NET-mediated inflammation of the vasculature: activation of emergency granulopoiesis via granulocyte colony-stimulating factor production and induction of the endothelial cytoadhesion receptor intercellular adhesion molecule–1. Soluble NET components facilitate parasite sequestration and mediate tissue destruction. We demonstrate that neutrophils have a key role in malaria immunopathology and propose inhibition of NETs as a treatment strategy in vascular infections.

INTRODUCTION

Neutrophils are the most abundant leukocytes in the blood, and they respond to pathogens by phagocytosis, generation of oxidants, and externalization of microbicidal peptides and proteases (*1*). The release of these compartmentalized antimicrobials is achieved by either degranulation or the release of neutrophil extracellular traps (NETs). NETs consist of decondensed chromatin decorated with microbicidal and immunostimulatory molecules (*2*, *3*). NETs are released by a cell death program termed "NETosis," and they ensure high local concentrations of active antimicrobials. Eventually, deoxyribonuclease 1 (DNase 1), a constitutive plasma endonuclease, degrades NETs and facilitates their removal (*4*).

NETosis is an active process that requires microbial or mitogenic signaling (*5*, *6)*; the production of reactive oxygen species (ROS) (*7*); the activity of two serine proteases, neutrophil elastase (NE) and proteinase 3 (PR3) (*8*, *9*); and the activation of the pore-forming protein gasdermin D (*10*). NE translocates from the granules to the nucleus during NET induction, where it cleaves histones to allow chromatin decondensation before plasma membrane breakdown (*8*). NE and PR3 have partially overlapping substrates (*11*) and are both required for maximal NET induction in vivo (*9*).

Triggering of NETosis by various microbes in tissues or the mucosa limits pathogen proliferation and dissemination (*12*). NET release inside the vasculature, however, can be pathogenic by triggering autoimmunity (*13*), as well as by directly damaging blood vessels (*14*, *15*) and inducing thrombosis (*16*).

To understand the role of neutrophils and NETs in intravascular infections, we investigated malaria, a disease caused by protozoan parasites that invade red blood cells (RBCs) and trigger systemic neutrophil activation (*17*, *18*). *Plasmodium falciparum* is the most important and virulent species, causing more than 200 million malaria episodes and close to 500,000 deaths annually (*19*). It encompasses diverse pathological manifestations that can range from mild non-specific symptoms, fever, and mild anemia to organ failure, acidosis, coma, and death. Complications of severe malaria include coma, prostration, respiratory distress, metabolic acidosis, renal failure, liver damage, and severe anemia (*20*, *21*).

Pathogenesis of *P. falciparum* malaria is precipitated by its interaction with the vascular endothelium. In the second half of the asexual erythrocytic life cycle, parasites express cytoadhesion factors on the surface of infected RBCs (iRBCs), allowing binding and sequestration in postcapillary venules. Attachment and withdrawal from circulation are thought to aid in preventing clearance of iRBCs by splenic macrophages (*22*). Disease severity is synergistically determined by sequestration patterns and host inflammatory responses (*23*, *24*). Cytoadhesion of iRBCs leads to endothelial activation and vascular occlusion (*24*), whereas release of pathogen- or danger-associated molecular pattern (PAMP or DAMP, respectively) molecules leads to pathological inflammatory responses mediated by cytokines such as tumor necrosis factor–α (TNF-α) and interleukin-1β (IL-1β) (*25*). Organ-specific iRBC sequestration is associated with corresponding pathology (*23*, *24*).

Despite the important inflammatory component of the disease, the role of neutrophils in *P. falciparum* malaria remains unclear. Neutrophils isolated from patients with malaria have a reduced capacity to mount an oxidative burst (*26*). On the other hand, several

[1]Max Planck Institute for Infection Biology, Department of Cellular Microbiology, Charitéplatz 1, 10117 Berlin, Germany. [2]Section of Paediatrics, Imperial College London, London W21 PG, UK. [3]Max Planck Institute for Infection Biology, Microscopy Core Facility, Charitéplatz 1, 10117 Berlin, Germany. [4]Wellcome Centre for Integrative Parasitology, Institute of Infection, Immunity and Inflammation, University of Glasgow, Glasgow, UK. [5]Institute of Infection and Global Health, University of Liverpool, 8 West Derby Street, Liverpool L69 7BE, UK. [6]Francis Crick Institute, 1 Midland Road, London NW1 1AT, UK. [7]Charité—Universitätsmedizin Berlin, Humboldt-Universität zu Berlin, and Berlin Institute of Health, Department of Pediatric Pneumology, Immunology and Intensive Care, Berlin, Germany. [8]Department of Eye and Vision Science, Institute of Ageing and Chronic Disease, University of Liverpool, Liverpool, UK. [9]Stavanger University Hospital, Stavanger, Norway. [10]Maputo Central Hospital, Maputo, Mozambique. [11]Research Institute of Internal Medicine, Oslo University Hospital Rikshospitalet, Oslo, Norway. [12]Centre de Recherches Médicales de Lambaréné (CERMEL), Lambaréné, Gabon. [13]Universität Tübingen, Institut für Tropenmedizin, Wilhelmstraße 27, 72074 Tübingen, Germany. [14]Department of Oncology, University of Turin, Via Santena 5 bis, 10126 Turin, Italy. [15]University of Bristol, School of Cellular and Molecular Medicine, Bristol BS8 1TD, UK.
*Corresponding author. Email: borko.amulic@bristol.ac.uk

studies have linked activation of these cells to pathogenesis and severe disease (*17*, *18*, *27*). For instance, a recent blood transcriptomic analysis comparing severe and uncomplicated malaria identified a granulocyte colony-stimulating factor (G-CSF)–regulated neutrophil granulopoiesis signature as a specific feature of severe malaria (*18*). Granulopoiesis refers to production of neutrophils from progenitor cells in the bone marrow; this blood signature therefore identifies increased neutrophil abundance as a pathogenic factor in malaria. Furthermore, genes encoding neutrophil granule proteins, such as NE and matrix metalloproteinase–8, showed the highest up-regulation between severe and uncomplicated malaria (*18*). Similarly, a study in Malawi demonstrated that retinopathy-positive cerebral malaria (CM) is specifically associated with accumulation of externalized neutrophil proteins such as NE and PR3 (*17*). Several studies in mice have also linked neutrophils to severe malaria (*28*–*31*). Depletion of neutrophils with anti-Ly6G antibody reduces pathology in *Plasmodium chabaudi chabaudi* mouse infections (*28*).

In addition to the accumulation of soluble neutrophil proteases, severe disease is associated with an increase in extracellular human nucleosomes in patients' plasma (*32*), which could indicate NET release. NETs are a platform for externalizing both nucleosomes and neutrophil proteases and could thus be an important pathogenic factor in malaria. NETs were reported in mouse malaria (*31*) and NET-like structures were observed on patient blood smears (*33*, *34*).

We show, using patient samples, that NETs are triggered by extracellular heme in malaria. We found NETs to be a source of immunostimulatory molecules—alarmins—that activate emergency hematopoiesis via G-CSF induction. In the *P. chabaudi* mouse model, host DNase 1 liberated neutrophil proteins from NETs, and this release was required for neutrophilia and neutrophil infiltration in the liver. Soluble NET components were also required for parasite sequestration in the liver and the lung. Genetic depletion of NETs or NET-processing DNase 1 reduced organ damage. We demonstrate an undescribed physiological role for circulating NETs and identify a potential target for adjunctive malaria therapy.

RESULTS

Intravascular NETs are formed in *P. falciparum* malaria

To test whether *P. falciparum* malaria is accompanied by bona fide NET induction, we initially analyzed plasma samples from 43 parasitologically confirmed pediatric and adult patients, treated at the Albert Schweitzer Hospital, in Lambaréné, Gabon, a highly malaria-endemic region in Central Africa. The patients presented with variable symptoms such as hyperparasitemia, fever, and anemia (table S1) but did not show severe symptoms and all recovered upon antimalarial treatment. NETs are defined as complexes of chromatin and neutrophil granule proteins; hence, we used an enzyme-linked immunosorbent assay (ELISA) that detects NETs with an anti-DNA detection antibody, preceded by a capture antibody against NE. Patients with malaria had significantly elevated levels of NETs compared with healthy controls from the same region ($n = 9$) (Fig. 1A).

To test whether NETs are linked to malaria severity, we next measured NE-DNA complexes in plasma from two different patient cohorts, each consisting of uncomplicated and severe malaria. The first cohort again consisted of pediatric patients from Lambaréné, Gabon, recruited in 1995 and 1996 as part of a case-control study with a subsequent longitudinal survey comparing severe ($n = 23$) with strictly defined uncomplicated malaria cases ($n = 10$; table S2). Most children had severe anemia or hyperparasitemia and other complications; mortality was 3% (*35*). The second cohort consisted of HIV-negative adult in-patients at the Central Hospital in Maputo, Mozambique, 28 of whom had uncomplicated malaria and 27 had severe malaria. Severe malaria in this cohort was defined according to the severity criteria developed by the World Health Organization (*36*) and included CM, respiratory distress, liver failure, and severe anemia (table S2). In both cohorts, NETs were significantly enriched in severe versus uncomplicated malaria (Fig. 1, B and C).

We also isolated peripheral blood neutrophils from hospitalized adult patients and monitored NET formation. Neutrophils from patients with malaria ($n = 8$) released twofold more NETs than healthy controls ($n = 6$) (Fig. 1D). NETs were released without the addition of exogenous stimuli, indicating that NETosis in malaria is activated in vivo.

To further demonstrate NETs in vivo and to examine their association with neurovascular sequestration of iRBCs, a key event in CM pathogenesis, we examined retinal tissue from fatal pediatric patients who had died with a clinical diagnosis of CM. Retinopathy is a highly specific feature of CM (*37*), and pathological changes in the retinal vasculature in CM are representative of those in the cerebral microvasculature (*38*, *39*). Through postmortem examination, cases were divided into those who had sequestration of parasitized erythrocytes in the brain and no alternative cause of death and were deemed to have "true" CM and those who had no sequestration and were all found to have alternative causes of death. This second "faux CM" group is a useful comparator group to control the effect of fatal encephalopathy and premorbid events versus those that are due to parasite sequestration. We analyzed the retinas of nine definitive CM cases and eight comatose malaria cases without retinopathy (table S3) and identified NETs by colocalization of citrullinated histone H3, elastase, and DAPI (4′,6-diamidino-2-phenylindole). As expected, most of the retinal capillaries in true CM cases were packed with sequestered parasitized RBCs (Fig. 1E). NETosis was detected exclusively in retinopathy-positive CM cases (nine of nine) and localized only to areas with parasitized RBCs (Fig. 1, F and G). *Z*-stack imaging revealed that NETs filled the lumen of retinal capillaries (Fig. 1G), enveloping the parasitized erythrocytes. Together, these data demonstrate that NETs are induced in the vasculature of patients with malaria and that this correlates with parasite sequestration and disease severity.

NETs in malaria are induced by heme and TNF-α

To identify factors that trigger NET formation in malaria, we coincubated neutrophils from healthy adult donors with *P. falciparum* cultures. Neutrophils were either primed with TNF-α, a major malaria-associated proinflammatory cytokine (*24*), or left unprimed. We exposed neutrophils to iRBCs, free merozoites, and parasite digestive vacuoles (DVs), which are released upon RBC rupture and contain the hemozoin crystal, as well as heme, a known malaria DAMP that is released during parasite egress, as well as during "bystander hemolysis"—the inflammatory destruction of uninfected RBCs (*25*, *26*). Only heme robustly induced NETs in combination with TNF-α priming (Fig. 2A and fig. S1A), as previously reported in sickle cell disease (*40*).

To verify that NET formation is linked to hemolysis in vivo, we determined the plasma-free heme concentrations in our patient cohorts and examined their association with plasma NE-DNA complexes. We found that free heme positively correlates with circulating NETs in both Gabon cohorts (Fig. 2, B and C) but not in the adult Mozambique

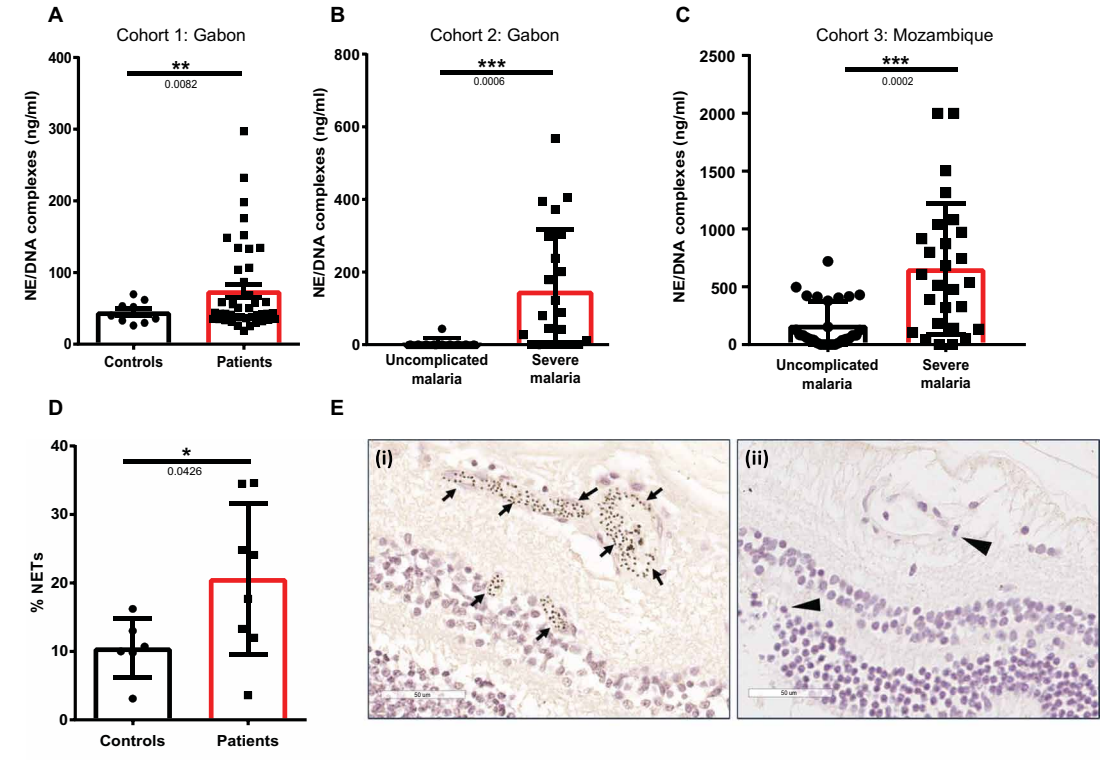

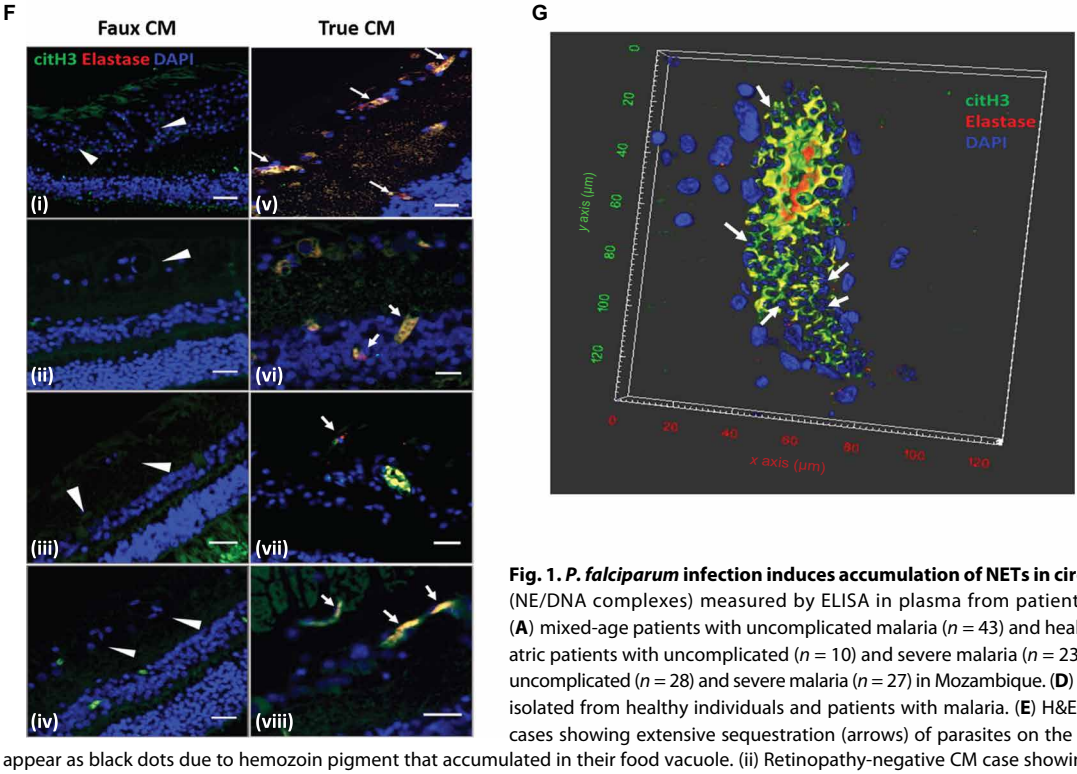

Fig. 1. *P. falciparum* infection induces accumulation of NETs in circulation. Circulating NET components (NE/DNA complexes) measured by ELISA in plasma from patients in three different malaria cohorts: (**A**) mixed-age patients with uncomplicated malaria ($n = 43$) and healthy controls in Gabon ($n = 9$), (**B**) pediatric patients with uncomplicated ($n = 10$) and severe malaria ($n = 23$) in Gabon, and (**C**) adult patients with uncomplicated ($n = 28$) and severe malaria ($n = 27$) in Mozambique. (**D**) Quantification of NETosis in neutrophils isolated from healthy individuals and patients with malaria. (**E**) H&E images of (i) retinopathy-positive CM cases showing extensive sequestration (arrows) of parasites on the retinal endothelium. Mature parasites appear as black dots due to hemozoin pigment that accumulated in their food vacuole. (ii) Retinopathy-negative CM case showing no sequestration in the vasculature (arrowheads point to the capillaries). Scale bars, 50 µm. (**F**) Merged images stained with citrullinated histone H3 (citH3; green), elastase (red), and DAPI (blue). Arrows indicate NETs, visualized by colocalization of all the stained components. Arrowheads point to the capillaries of retinopathy-negative cases that show no sequestration. Scale bars, 25 µm. Figure shows representative images from nine different "true" CM and eight different "faux" CM cases. (**G**) 3D reconstruction of capillary with very high sequestration by *Z*-stack images collected from a true CM case. Merged image with citrullinated histone H3 (green), elastase (red), and DAPI (blue). DAPI stains the parasite DNA inside the parasitized erythrocytes (arrows), as well as the nuclei of the host cells. Data are presented as mean ± SEM. Asterisks indicate significance: $^{*}P < 0.05$, $^{**}P < 0.01$, $^{***}P < 0.001$ by Welch's *t* test or Mann-Whitney test.

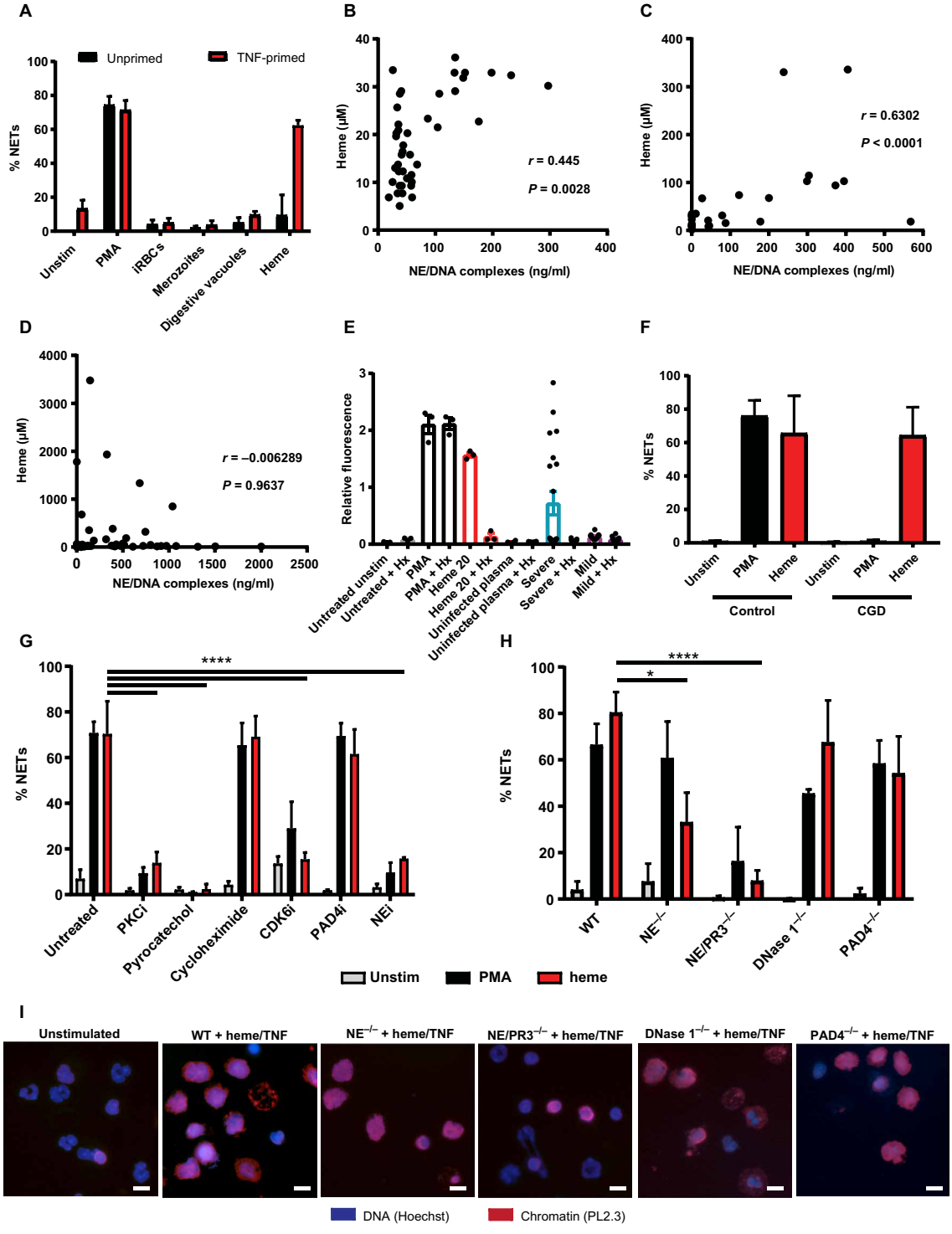

Fig. 2. Heme induces NETs in a mechanism requiring serine proteases. (**A**) In vitro stimulation of neutrophils isolated from healthy individuals ($n = 3$) with malaria-associated PAMPs and DAMPs ($n = 3$). (**B** to **D**) Spearman correlation of NETs and heme concentration in patients with malaria of all three cohorts presented in Fig. 1. (**E**) Quantification of NETosis of healthy neutrophils in response to plasma (10% v/v) from patients with malaria, PMA (50 nM), or heme (20 μM) in combination with TNF-α priming. Hx refers to treatment with 70 μM hemopexin for 30 min before stimulation. (**F**) Quantification of NETosis in neutrophils from healthy donors ($n = 3$) and patients with CGD ($n = 3$) in response to PMA and heme. (**G**) Quantification of NETosis in response to PMA and heme in neutrophils from healthy donors ($n = 3$) preincubated with inhibitors at the following concentrations: 1 μM Go6983 (PKCi), 30 uM pyrocatechol, cycloheximide (1 μg/ml), 2.5 μM abemaciclib (CDK6i), 10 μM BB-Cl-amidine (PAD4i), and 20 μM GW311616A (NEi). (**H**) Quantification of NET formation in mouse peritoneal neutrophils ($n = 3$) in response to PMA (100 nM) and heme (20 μM) with TNF-α pretreatment. (F to H) All graphs display mean ± SEM. (**I**) Representative images used for mouse NET quantifications, showing staining for DNA (blue) and histone H2A/H2B-DNA (red). Scale bars, 20 μm. Asterisks indicate significance: *$P < 0.05$, **$P < 0.01$, ***$P < 0.001$, and ****$P < 0.0001$ by two-way analysis of variance (ANOVA).

patients (Fig. 2D), possibly due to some very high heme values in the latter. Consequently, we incubated neutrophils from healthy donors with plasma from patients to test whether soluble factors are sufficient to induce NETs. Plasma from severe but not from mild malaria was sufficient to induce NETs in healthy neutrophils, and this effect was abolished by the heme scavenger hemopexin (Fig. 2E). In summary, accumulation of free heme during malaria activates neutrophils to release NETs.

Heme-induced NETs require oxidants and NE/PR3-mediated proteolysis

There are different pathways leading to NET formation (*41*). We tested the involvement of host factors previously implicated in NETosis, starting with the ROS-producing enzyme NOX2 (*7*). We isolated neutrophils from patients with chronic granulomatous disease (CGD) ($n = 3$), who carry NOX2 mutations, rendering them completely deficient in ROS production (fig. S1C). Heme induced similar levels of NETs in CGD and control neutrophils unlike the phorbol ester phorbol 12-myristate 13-acetate (PMA), which failed to induce NETs in CGD cells (Fig. 2F). Although this oxidase was not involved, heme-induced NETs required ROS signaling because treatment with the ROS scavenger pyrocatechol (fig. S1C) completely abolished NETosis (Fig. 2G), suggesting that heme itself might be the oxidizing agent. The requirement for ROS was confirmed with a second scavenger, *N*-acetylcysteine (NAC; fig. S1E). Heme required intracellular oxidant production because a combination of two non–cell-permeant scavengers, catalase, and superoxide dismutase, failed to block NETs, as did a scavenger of mitochondrial ROS (fig. S1E).

In addition to oxidants, heme-triggered NETs required activity of protein kinase C (PKC) (*42*), cyclin-dependent kinase 6 (CDK6) (*5*), and NE/PR3 (*9*) but were independent of peptidyl arginine deiminase 4 (PAD4)–mediated citrullination (*43*) (Fig. 2G). We also tested the requirement for de novo protein synthesis using the translational inhibitor cycloheximide. This drug, at a concentration that fully blocked synthesis of the cytokine IL-8 (fig. S1B), had no effect on NET formation (Fig. 2G), as previously reported for other NET-inducing stimuli (*44*).

To genetically confirm the role of proteases in heme NET induction, we purified peritoneal neutrophils from NE single-knockout and NE/PR3 double-knockout mice. NE/PR3$^{-/-}$ neutrophils failed to release extracellular chromatin, whereas NE$^{-/-}$ cells displayed a partial deficiency (Fig. 2, H and I), demonstrating that these proteases have an essential nonredundant function in decondensing chromatin. In contrast, there was no difference in NET formation between PAD4$^{-/-}$ and control neutrophils (Fig. 2, H and I).

NET fragments drive malaria pathology in vivo

To address the function of NETs in *Plasmodium* infections in vivo, we used NE/PR3$^{-/-}$ mice as a NET-deficient model. In addition, to investigate the effect of a failure to degrade NETs extracellularly, we used DNase 1$^{-/-}$ mice. In the absence of DNase 1, NETs are made normally (Fig. 2, H and I), but they persist at sites of release because they are not processed into soluble components (*4*). DNase 1$^{-/-}$ animals are deficient in dispersal of NET components and are a model to study the systemic effects of NET-associated alarmins.

We infected mice with the erythrocytic stages of *P. chabaudi*, a rodent malaria parasite that causes a nonlethal, 2-week acute infection. Similarly to *P. falciparum*, *P. chabaudi* iRBCs synchronously sequester in organs and induce pathology (*45*, *46*), although the sequestration patterns differ in the two species and different parasite-encoded proteins mediate cytoadhesion. We quantified NETs in plasma by detecting soluble complexes of DNA and the granule protein myeloperoxidase (MPO). We chose MPO over NE to enable us to analyze NETs in NE-deficient mice. NET components (Fig. 3A) and extracellular nucleosomes (Fig. 3B) increased in infected wild-type (WT) mice but were completely absent in NE/PR3 and DNase 1$^{-/-}$ mice. This result is consistent with a failure to produce NETs in the case of NE/PR3$^{-/-}$ animals and with a failure to break down the NET macrostructure in the case of DNase 1$^{-/-}$. Parasitemia was similar in all three mouse strains (Fig. 3C), showing that NETs are not antiparasitic. As previously described (*28*, *45*), parasitemia peaked between days 9 and 11 and was suppressed by day 13 after infection.

P. chabaudi sequesters in the liver and lungs where it induces tissue damage and immunopathology (*45*). Livers from WT mice were severely darkened and discolored because of the accumulation of hemozoin and hepatocyte death (Fig. 3D). Livers of infected NE/PR3$^{-/-}$ and DNase 1$^{-/-}$ mice were completely unaffected and indistinguishable from uninfected controls (Fig. 3D). Livers of WT, but not NE/PR3$^{-/-}$ or DNase1$^{-/-}$ mice, showed necrosis and immune infiltration, characteristic malaria pathology, upon histological analysis of hematoxylin and eosin (H&E)–stained sections (Fig. 3E and fig. S2, A and B). We confirmed the liver pathology in WT but not mutant mice, with the hepatic damage marker aspartate aminotransferase (AST) in plasma (Fig. 3F). Tissue damage was also reduced in lungs of NE/PR3$^{-/-}$ (fig. S3) compared with WT controls, although *P. chabaudi* causes only mild lung pathology (*45*). Together, these data demonstrate that release of components from NETs promotes organ pathology in malaria.

Exogenous NET components restore pathology in NET-deficient mice

To confirm that NETs are pathogenic in malaria, we injected mice with in vitro generated NET fragments. We chose NE/PR3$^{-/-}$ mice as the NET-deficient strain to carry out this complementation experiment. We first purified peritoneal neutrophils from WT mice and induced them to form NETs. After washing, NETs were dislodged by scraping and sonicated to obtain fragments, which were quantified on the basis of DNA content and injected into the tail vein of control and *P. chabaudi* parasitized mice. Injection of NET fragments did not cause liver pathology in uninfected mice (Fig. 3G), nor did it affect parasitemia in any of the infected genotypes (fig. S4). Restoring NET fragments in parasitized NE/PR3$^{-/-}$ mice fully recapitulated the liver damage observed in WT mice (Fig. 3G). This result demonstrates the direct pathogenicity of NETs and rules out a cell-intrinsic effect of proteases as the cause of the protective effect in the knockout animals.

NETs contain multiple components with inflammatory activity (*47*). These include the DNA backbone, as well as the protein fraction that contains many alarmins. Furthermore, extracellular nucleosomes and histones, which form a major portion of NETs, are inflammatory when found in the bloodstream (*48*). To identify which NET components are responsible for inducing pathology, we used recombinant DNase 1 to fully digest the DNA of the in vitro NET preparation, leaving only the protein components. The NET protein fraction was sufficient to induce liver damage in NE/PR3 null mice (Fig. 3G). As a control, we also injected mouse nucleosomes purified from bone marrow–derived macrophages, which failed to induce AST release after injection (Fig. 3G). These data show that the pathogenic activity derives from a NET-associated protein.

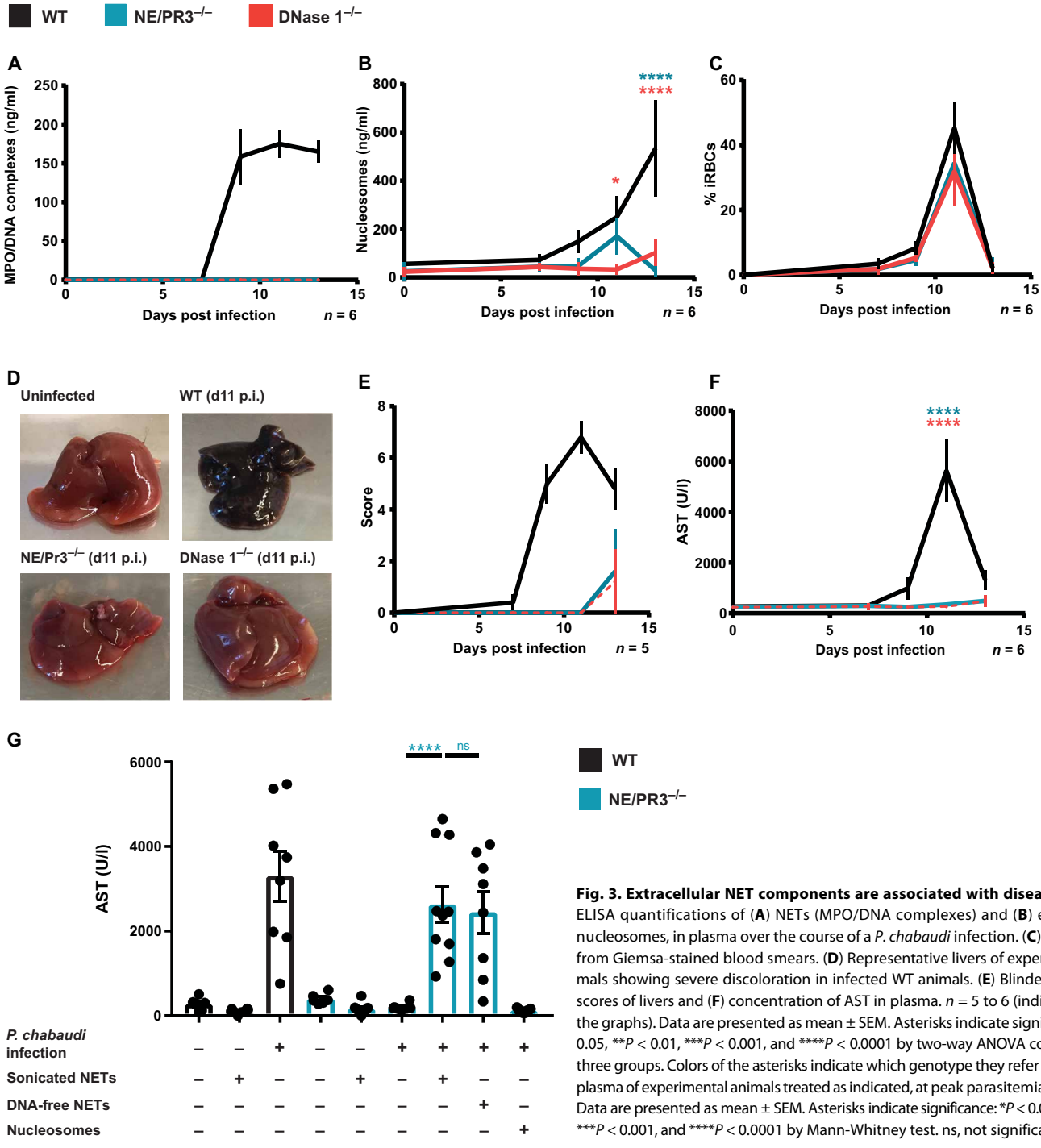

Fig. 3. Extracellular NET components are associated with disease severity. ELISA quantifications of (**A**) NETs (MPO/DNA complexes) and (**B**) extracellular nucleosomes, in plasma over the course of a *P. chabaudi* infection. (**C**) Parasitemia from Giemsa-stained blood smears. (**D**) Representative livers of experimental animals showing severe discoloration in infected WT animals. (**E**) Blinded pathology scores of livers and (**F**) concentration of AST in plasma. $n = 5$ to 6 (indicated under the graphs). Data are presented as mean ± SEM. Asterisks indicate significance: $^{*}P < 0.05$, $^{**}P < 0.01$, $^{***}P < 0.001$, and $^{****}P < 0.0001$ by two-way ANOVA comparison of three groups. Colors of the asterisks indicate which genotype they refer to. (**G**) AST in plasma of experimental animals treated as indicated, at peak parasitemia. $n = 6$ to 10. Data are presented as mean ± SEM. Asterisks indicate significance: $^{*}P < 0.05$, $^{**}P < 0.01$, $^{***}P < 0.001$, and $^{****}P < 0.0001$ by Mann-Whitney test. ns, not significant.

NETs induce emergency granulopoiesis via G-CSF induction

Neutrophils cause tissue destruction due to the cytotoxic molecules they carry. We quantified neutrophil infiltration into the livers of parasitized mice using immunofluorescence staining of the intracellular neutrophil marker calgranulin A. Neutrophils accumulated in the livers of WT, but not NE/PR3$^{-/-}$ and DNase 1$^{-/-}$ animals (Fig. 4A and fig. S5), consistent with neutrophils being initiators of hepatic pathology.

We quantified systemic neutrophil numbers to determine why both deficient mice genotypes failed to recruit neutrophils into the liver. In malaria, like other infections, the number of circulating neutrophils increases due to emergency granulopoiesis in the bone marrow (*49*–*51*). We observed that *P. chabaudi* infection leads to neutrophilia in WT mice but not in NE/PR3 and DNase1 knockouts (Fig. 4B).

The major mediator of emergency granulopoiesis is G-CSF (*52*). We speculated that NETs directly induce G-CSF. To test this, we stimulated macrophages—a significant physiological source of this cytokine—with NETs in vitro. NETs robustly induced production

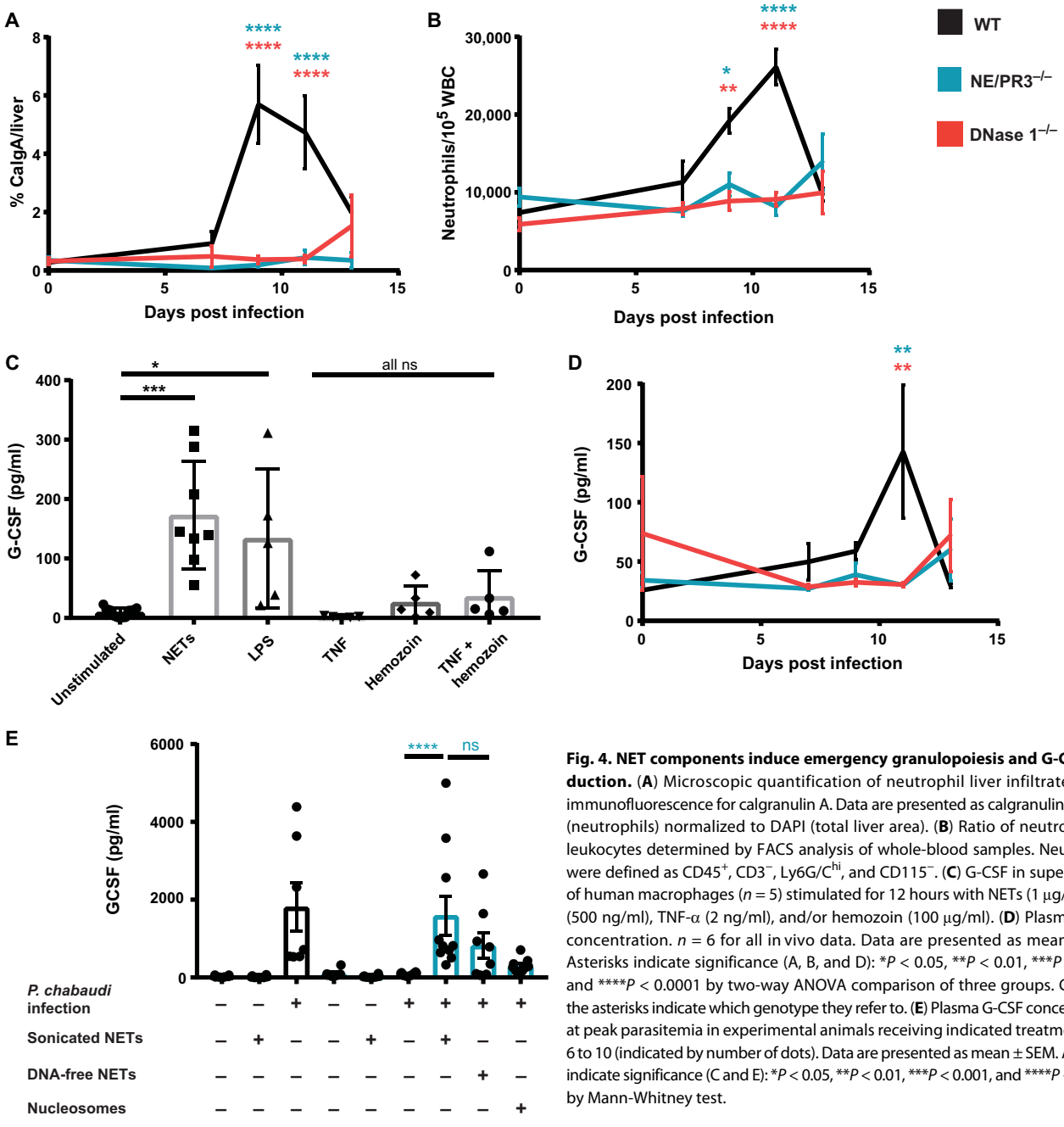

Fig. 4. NET components induce emergency granulopoiesis and G-CSF production. (**A**) Microscopic quantification of neutrophil liver infiltrates using immunofluorescence for calgranulin A. Data are presented as calgranulin A signal (neutrophils) normalized to DAPI (total liver area). (**B**) Ratio of neutrophils to leukocytes determined by FACS analysis of whole-blood samples. Neutrophils were defined as $CD45^+$, $CD3^-$, $Ly6G/C^{hi}$, and $CD115^-$. (**C**) G-CSF in supernatants of human macrophages ($n = 5$) stimulated for 12 hours with NETs (1 μg/ml), LPS (500 ng/ml), TNF-α (2 ng/ml), and/or hemozoin (100 μg/ml). (**D**) Plasma G-CSF concentration. $n = 6$ for all in vivo data. Data are presented as mean ± SEM. Asterisks indicate significance (A, B, and D): $^*P < 0.05$, $^{**}P < 0.01$, $^{***}P < 0.001$, and $^{****}P < 0.0001$ by two-way ANOVA comparison of three groups. Colors of the asterisks indicate which genotype they refer to. (**E**) Plasma G-CSF concentration at peak parasitemia in experimental animals receiving indicated treatments. $n =$ 6 to 10 (indicated by number of dots). Data are presented as mean ± SEM. Asterisks indicate significance (C and E): $^*P < 0.05$, $^{**}P < 0.01$, $^{***}P < 0.001$, and $^{****}P < 0.0001$ by Mann-Whitney test.

of G-CSF in human monocyte-derived macrophages, at levels similar to those obtained with bacterial lipopolysaccharide (LPS) and exceeding those obtained with TNF-α or hemozoin (Fig. 4C).

In *P. chabaudi*–infected WT mice, the concentration of G-CSF in plasma increased with rising parasitemia; however, there was no increase in either NE/PR3$^{-/-}$ or DNase 1$^{-/-}$ mice (Fig. 4D). To directly demonstrate that NETs induce G-CSF in vivo, we injected sonicated NETs as described before. Injection of NET fragments fully restored G-CSF production in NE/PR3 mice to levels seen in WT mice (Fig. 4E). As with the liver damage marker AST, G-CSF production was induced by the protein component of NETs because complete removal of DNA before injection did not abrogate the effect. These data show that NET-associated alarmins drive emergency hematopoiesis by inducing G-CSF release.

NETs promote parasite sequestration in organs

Malaria pathology is linked to parasite sequestration in the microvasculature of afflicted organs. The lack of discoloration in livers of infected NE/PR3$^{-/-}$ and DNase 1$^{-/-}$ mice (Fig. 3D) suggests a lack of parasite adhesion. To directly analyze sequestration, we infected mice with a luciferase-expressing strain of *P. chabaudi* (*45*) and quantified sequestered parasite load in organs, at the time of maximal cytoadhesion, after perfusing animals to remove unbound, freely circulating parasites.

As reported, *P. chabaudi* sequestered most prominently in the liver and the lung and, to a lesser degree, in the kidneys (*45*). There were 10-fold fewer parasites sequestered in the livers and lungs of NE/PR3$^{-/-}$ and DNase 1$^{-/-}$ mice compared with WT controls (Fig. 5A). We confirmed this sequestration pattern by histological enumeration of iRBCs in the liver microvasculature (Fig. 5B and fig. S2B), as well as by electron microscopy (fig. S2C).

NETs induce up-regulation of endothelial cytoadhesion receptors

The difference in abundance of neutrophils in livers of WT and knockout animals was greater than the difference observed in peripheral blood, indicating that, in addition to emergency granulopoiesis, NETs regulate neutrophil trafficking. Both neutrophils (*53*) and parasites (*54*, *55*) can use the same receptor [intercellular adhesion molecule–1 (ICAM-1)] to dock to endothelial cells. We hypothesized that NET components regulate expression of ICAM-1 on the endothelium. To test this, we analyzed ICAM-1 immunofluorescence in liver sections and observed up-regulation on endothelia of infected WT but not NE/PR3$^{-/-}$ or DNase1$^{-/-}$ mice, coinciding with the onset of liver damage (Fig. 5, C and D). We also measured soluble ICAM-1 in plasma as an additional readout for expression of this receptor and found no induction in NE/PR3$^{-/-}$ compared with WT animals (Fig. 5E), confirming our microscopy results. Injection of in vitro generated NET fragments into parasitized NE/PR3$^{-/-}$ mice restored the expression of ICAM-1 (Fig. 5E), demonstrating that NET components control ICAM-1 expression.

Parasitized erythrocytes can bind to multiple endothelial surface proteins. Another prominent cytoadhesion receptor is CD36 (*56*). We tested whether NETs control expression of CD36 by microscopically analyzing protein abundance in lung endothelia. Similarly to ICAM-1, CD36 immunofluorescence increased in lungs of infected mice, and this induction was absent in NE/PR3$^{-/-}$ animals (Fig. 5F). We confirmed this result by quantifying levels of CD36 in plasma (Fig. 5G). Contrary to what we observed with ICAM-1, injection of NETs into uninfected mice was sufficient to up-regulate CD36 (Fig. 5F). In summary, NET-associated proteins facilitate iRBC sequestration by inducing endothelial activation.

Neutralizing G-CSF antibodies decrease liver damage

To test whether G-CSF–induced neutrophilia is pathogenic, we neutralized the effects of this cytokine by injecting parasitized animals with an anti–G-CSF antibody, at day 7 after infection. As expected, the neutralizing antibody did not affect parasite burden (Fig. 6A), but it decreased circulating neutrophils compared with the isotype control (Fig. 6B). This also significantly reduced circulating NET components (Fig. 6C), as well as neutrophil trafficking into the liver (Fig. 6D). G-CSF neutralization diminished both parasite sequestration (Fig. 6E) and liver damage (Fig. 6F), providing a proof of principle that neutrophils can be successfully targeted in *Plasmodium* infection. The G-CSF concentration in plasma of patients with malaria is significantly increased in infected individuals (Fig. 6G), as previously reported (*57*).

DISCUSSION

Malaria pathophysiology is based on an interplay of parasite proliferation, host inflammatory response, and microvascular obstruction due to binding of iRBCs to activated endothelia. Despite important recent advances (*17*, *18*, *58*), the contribution of neutrophils to these processes remains poorly understood. Here, we demonstrate that neutrophils play an essential role in both propagation of inflammation and facilitation of parasite cytoadherence.

First, we showed that, in malaria, as in sickle cell disease (*40*), extracellular heme triggers NETosis in TNF-α–primed neutrophils. Heme-induced NETs require some of the same signaling intermediates demonstrated for other NET inducers, including neutrophil proteases (*8*), CDK6 (*5*), and PKC (*42*). Heme was previously shown to activate PKC in neutrophils, initiating chemotaxis and IL-8 production (*59*). TNF-α priming provides a synergistic signal required for NETosis; this signal is posttranslational because it is not blocked by the translational inhibitor cycloheximide. Heme-induced NETs are independent of the citrullinating enzyme PAD4, which is implicated in ionophore-induced NETs (*43*) and of the oxidant-generating enzyme NOX2 (*41*), which is known to be suppressed in neutrophils from patients with malaria (*26*). ROS signaling is nevertheless required for heme NETs because the response is blocked by the ROS scavenger pyrocatechol. This may be due to the fact that heme itself is a redox-active molecule with multiple mechanisms for initiating and propagating free radicals (*60*). In summary, heme uses a unique pathway for NET induction that nevertheless requires both protease activity and ROS signaling.

NETs are essential for malaria pathology in the *P. chabaudi* model. We showed that solubilization of NETs by serum DNase 1 liberates immunostimulatory components that diffuse systemically and are pathogenic via two mechanisms. The first is induction of G-CSF in macrophages, which initiates emergency granulopoiesis. This corresponds to what is seen in patients, where G-CSF is elevated in both *P. falciparum* (*57*) and *Plasmodium vivax* infections (*61*). Moreover, neutrophil turnover is often higher in malaria (*49*–*51*), and, in children living in endemic areas, increased neutrophil counts correlate with symptoms of severe disease, such as prostration, coma, and respiratory distress (*62*–*64*). In a second mechanism, NET components up-regulate mouse ICAM-1, a key cytoadhesion receptor that sequesters parasitized RBCs in the microvasculature of both mice and patients (*54*, *55*). In *P. falciparum* malaria, ICAM-1 mediates cytoadhesion in the brain and is a key mediator of CM (*55*, *65*). Antibodies against ICAM-1 binding variants of *P. falciparum* erythrocyte membrane protein 1 (PfEMP1), the main parasite cytoadhesion factor, protect against clinical disease (*66*, *67*). NET induction of ICAM-1, which facilitates *P. chabaudi* adhesion in the liver, may thus operate in human malaria to recruit *P. falciparum* iRBCs to the brain, a far more dangerous sequestration site. This is consistent with recent reports showing an association between neutrophil proteins and CM (*17*, *18*). Whether NETs can also up-regulate ICAM-1 on human brain endothelium remains to be verified.

NET components are also required for pathology and parasite sequestration in the lungs of infected animals, demonstrating that this mechanism may be broadly generalizable to different vascular beds. Furthermore, in the *P. chabaudi* model, lung sequestration is mediated by an unidentified receptor other than ICAM-1 (*54*), consistent with NET components inducing more than one cytoadhesion molecule. It will be interesting to test whether a similar mechanism operates in humans because neutrophils are known to infiltrate the lungs of patients with malaria with acute respiratory distress (*68*).

Our data demonstrate the essential role of DNase 1 in releasing pathogenic NET fragments in *P. chabaudi* malaria. NETs are thought to be anchored to the endothelium after release (*69*, *70*), through

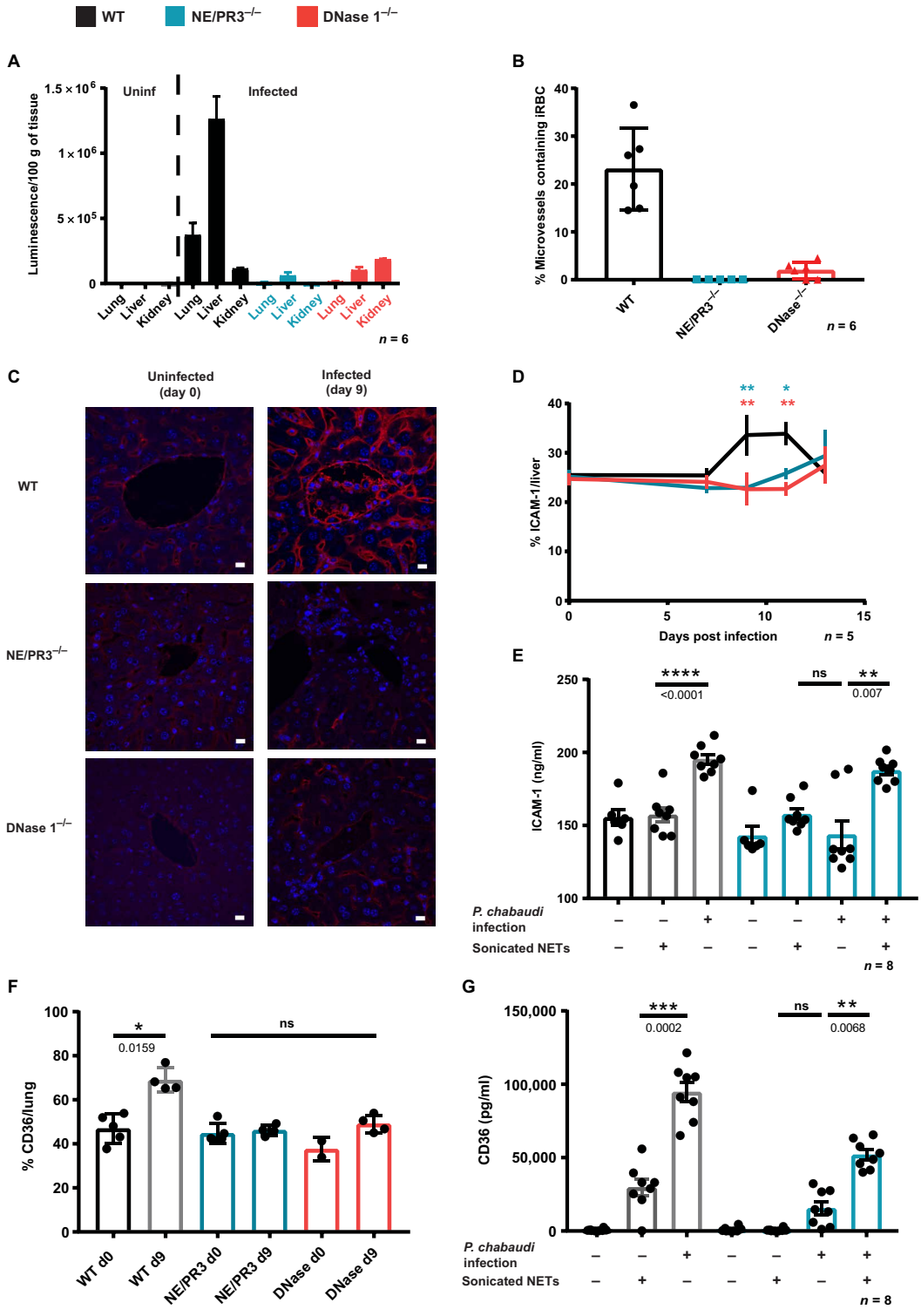

Fig. 5. NETs promote parasite sequestration and endothelial activation. (**A**) Parasite sequestration in different organs measured by quantification of luminescence from a luciferase-expressing strain of *P. chabaudi* ($n = 6$ mice). (**B**) Histological quantification of parasites sequestered in the microvasculature of the liver from H&E images ($n = 6$). (**C**) Representative images of immunofluorescence staining of ICAM-1 (red) and DNA (blue) in the livers of experimental animals. (**D**) Quantification of ICAM-1 signal from (C), normalized to DAPI (total liver area; $n = 6$). (**E**) Soluble ICAM-1 in plasma of experimental animals treated as indicated ($n = 8$). (**F**) Immunofluorescence microscopy quantification of CD36 expression in lung sections, normalized to DAPI signal [total lung area; $n = 2$ to 5 (indicated by number of dots)]. (**G**) CD36 concentration in plasma measured by ELISA ($n = 8$). Data are presented as mean ± SEM. Asterisks indicate significance. (D) $^*P < 0.05$, $^{**}P < 0.01$, $^{***}P < 0.001$, and $^{****}P < 0.0001$ by two-way ANOVA comparison of three groups. Colors of the asterisks indicate which genotype they refer to. (E to G) $^*P < 0.05$, $^{**}P < 0.01$, $^{***}P < 0.001$, and $^{****}P < 0.0001$ by Mann-Whitney test.

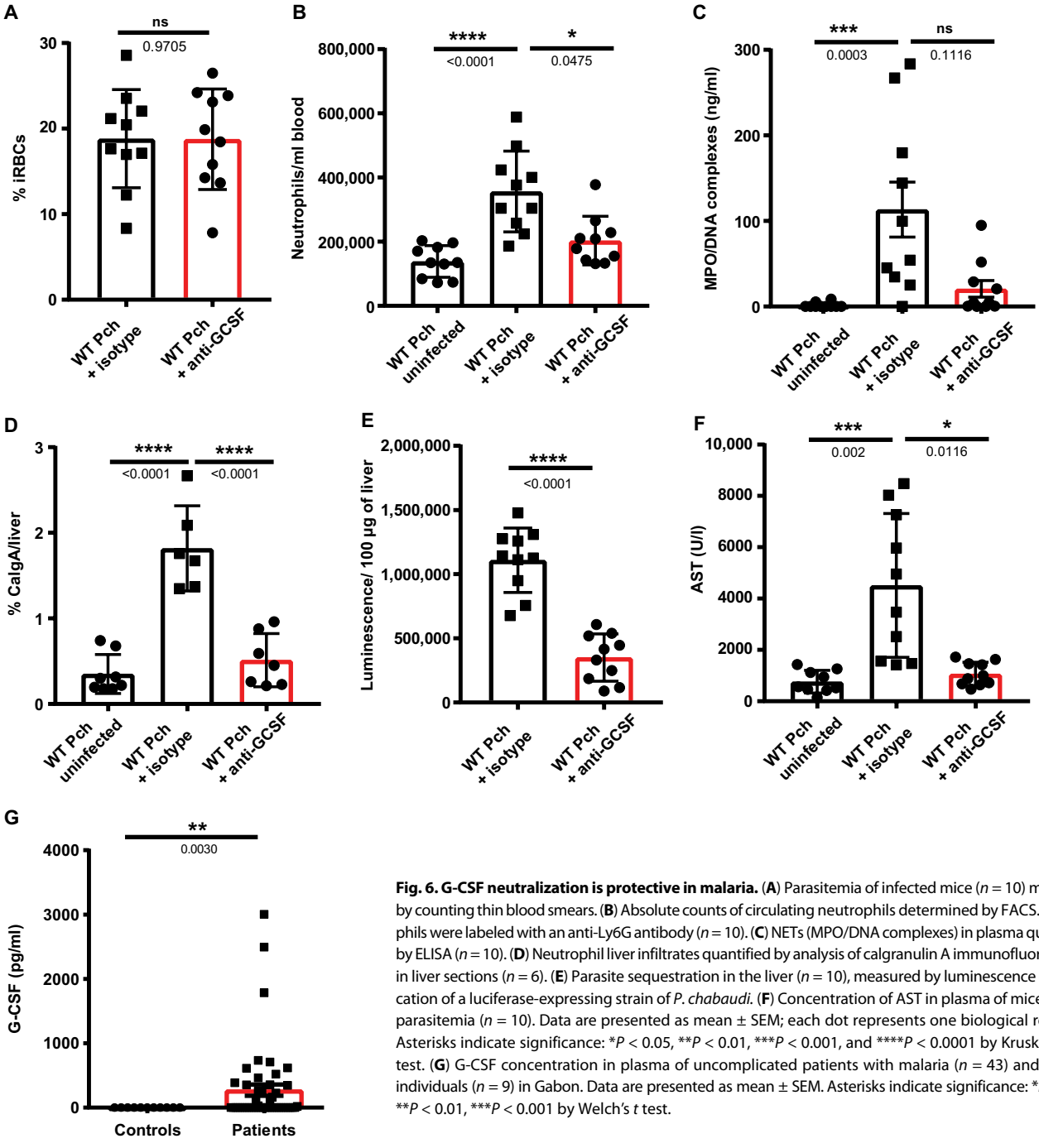

Fig. 6. G-CSF neutralization is protective in malaria. (**A**) Parasitemia of infected mice ($n = 10$) measured by counting thin blood smears. (**B**) Absolute counts of circulating neutrophils determined by FACS. Neutrophils were labeled with an anti-Ly6G antibody ($n = 10$). (**C**) NETs (MPO/DNA complexes) in plasma quantified by ELISA ($n = 10$). (**D**) Neutrophil liver infiltrates quantified by analysis of calgranulin A immunofluorescence in liver sections ($n = 6$). (**E**) Parasite sequestration in the liver ($n = 10$), measured by luminescence quantification of a luciferase-expressing strain of *P. chabaudi*. (**F**) Concentration of AST in plasma of mice at peak parasitemia ($n = 10$). Data are presented as mean ± SEM; each dot represents one biological replicate. Asterisks indicate significance: $^{*}P < 0.05$, $^{**}P < 0.01$, $^{***}P < 0.001$, and $^{****}P < 0.0001$ by Kruskal-Wallis test. (**G**) G-CSF concentration in plasma of uncomplicated patients with malaria ($n = 43$) and healthy individuals ($n = 9$) in Gabon. Data are presented as mean ± SEM. Asterisks indicate significance: $^{*}P < 0.05$, $^{**}P < 0.01$, $^{***}P < 0.001$ by Welch's *t* test.

von Willebrand factor (*69*) and probably other mediators. Serum DNase 1 allows systemic diffusion of NET components, as demonstrated by the absence of NET fragments in DNase 1 knockouts. A similar pathogenic function of DNase 1 was shown in a polymicrobial sepsis model, where injection of recombinant DNase 1 promotes liver damage and neutrophil accumulation in the liver and lung (*71*). However, DNase 1 has contradictory roles in inflammation: In thrombosis (*72*, *73*), cancer (*74*), and SLE (*4*), this endonuclease is protective rather than pathogenic. In sterile inflammation, it is therefore the unprocessed NET "macrostructure" that is detrimental, whereas in infections such as malaria and sepsis, it is the discrete molecular components of NETs that cause disease.

The NET proteins that induce G-CSF and ICAM-1 remain unknown. Many proteins found on NETs are classified as alarmins (*75*), including α-defensins, cathelicidin, calgranulin, and lactoferrin (*76*). Once released, these alarmins can induce the maturation and activation of dendritic cells, T cells, macrophages, and endothelial cells (*75*). Additional experiments will determine which NET-bound proteins are responsible for triggering granulopoiesis and endothelial activation.

Table 1. Hepatitis (malaria).

Histopathologic changes	Histopathologic grading			
	0	1	2	3
Fatty change	No fatty change	<10%	10–50%	>50%
Kupffer cells/high power field (HPF)	<20/HPF	20–35/HPF	36–50/HPF	>50/HPF
Portal tract inflammation	<5% of portal tract area	5–15% of portal tract area	16–30% of portal tract area	>30% of portal tract area
Bile duct proliferation	No proliferation	Mild proliferation	Moderate proliferation	Severe proliferation
Sinusoid congestion	No congestion	Mild congestion	Moderate congestion	Severe congestion
Hemozoin deposition	No deposition	Mild deposition	Moderate deposition	Severe deposition
Necrosis	None	<10%	11–25%	>25%

Table 2. Acute lung injury.

0: Thin and delicate alveolar septae, no intra-alveolar fibrin strands or hyaline membranes, and <5 intra-alveolar cells, no perivascular, or peribronchial infiltrates

1: Mildly congested alveolar septae, few fibrin strands or hyaline membranes, and <10 intra-alveolar cells with mild perivascular and/or peribronchial infiltration

2: Moderately congested alveolar septae, some fibrin strands or hyaline membranes, <20 intra-alveolar cells with moderate perivascular, and/or peribronchial infiltration

3: Severely congested alveolar septae, many fibrin strands and presence of hyaline membranes, >20 intra-alveolar cells with severe perivascular, and/or peribronchial infiltration

NET-associated molecules are necessary but not sufficient to drive inflammation in *P. chabaudi* malaria, as shown by the injection of NET fragments into uninfected mice. Additional stimuli, most likely *Plasmodium* PAMPs, are required to initiate emergency hematopoiesis and liver damage. Although parasite proteins and hemozoin did not directly induce NETs, they are known to significantly contribute to immune activation via other pathways (*25*). Furthermore, inflammation in malaria is complex with type I interferons (*28*), $CD8^+$ T cells (*21*, *45*), and hemostasis (*77*) contributing to immunopathogenesis in both mice and humans. Further investigation is required to understand how neutrophils cross-talk with other cell types in initiating disease.

Malaria exerts an evolutionary selective pressure on populations living in endemic areas, selecting for gene variants that promote tolerance (*78*). People of African descent and some ethnic groups from the Middle East have low neutrophil counts (*79*). This "ethnic or benign neutropenia" could be the result of selective pressure to suppress neutrophil counts because they are detrimental in this disease. In addition to Duffy antigen, the loci linked to ethnic neutropenias include CDK6 and *GCSF* (*80*), both of which are directly involved in the NET-mediated pathogenic mechanism described here.

Recent studies confirmed the central role of heme in the pathophysiology of malaria (*81*, *82*). Moreover, extracellular heme accumulation is not limited to malaria; it is a confirmed pathogenic factor in sepsis, sickle cell disease, intracerebral hemorrhage, and atherosclerosis (*60*), all of which also have reported neutrophil involvement. It will therefore be interesting to examine whether emergency hematopoiesis and endothelial activation triggered by NET fragments are universal outcomes in intravascular hemolytic diseases.

Adjunctive therapies that treat the life-threatening complications of malaria are urgently needed. We show that NETs control inflammation and parasite cytoadherence, placing neutrophils at the nexus of malaria pathophysiology and identifying them as a potential target for adjunctive therapy.

MATERIALS AND METHODS

Study Design

This study uses ELISA of patient plasma samples and microscopy of retinal biopsies to examine a link between NETs and malaria pathogenesis. We use in vitro NET assays with human neutrophils to identify the factors responsible for NET induction in malaria and then test the consequences of NET deficiency by monitoring clinical signs in a mouse *P. chabaudi* infection model. Furthermore, we use flow cytometry, immunohistochemistry, ELISA, and in vivo sequestration assays of transgenic *P. chabaudi* parasites to test the involvement of NETs in granulopoiesis and parasite cytoadhesion in WT and NET-deficient mice.

Human samples

Our study was conducted in accordance with the Helsinki Declaration. Blood collection from healthy donors and patients with CGD was approved by the ethical committee of Charité University Hospital (Berlin, Germany). Collection of blood from patients with malaria in Gabon was approved by the Comité d'Ethique Régional Indépendent de Lambaréné in Gabon. All study participants provided written informed consent before being enrolled in the study.

Collection of blood samples from patients in Mozambique was approved by the Bioethical Committee in Mozambique and by the Regional Ethical Committee for Medical and Health Research Ethics in Eastern Norway. This study was previously described (*83*) and consisted of patients admitted to the Central Hospital of Maputo, Mozambique, during two malaria peak seasons from 2011 to 2012. Inclusion criteria were age ≥18 years, nonpregnancy, axillary temperature ≥38°C, confirmed malaria infection, and informed written/fingerprint consent from patient or next of kin.

Ethical approval to obtain, store, and use postmortem human tissue from Malawian children with fatal CM and non-CM encephalopathy was obtained from the research ethics committees at the College of Medicine Malawi, Liverpool School of Tropical Medicine, and Michigan State University. Informed consent was obtained from the parents or legal guardians of all the children enrolled.

Chemicals and stimuli

PMA (P8139, Sigma), heme (H651-9, Frontier Scientific), murine TNF-α (315-01A, PeproTech), human TNF-α (300-01A, PeproTech), PKC inhibitor (Go6976, Tocris Bioscience), pyrocatechol (C9510, Sigma), Hoechst 33342 (639, ImmunoChemistry Technologies), cycloheximide (Sigma), Cdk4/6 inhibitor (LY2835219, Selleck Chemicals), PAD4 inhibitor (TDFA, Tocris Bioscience), NE inhibitor (GW311616A, Sigma-Aldrich), luminol (11050, AAT Bioquest), horseradish peroxidase (31941, Serva), and Bright-Glo Luciferase substrate (E2610, Promega) were used in the study.

Immunofluorescence microscopy on human retinal tissue

Paraffin sections (3 to 4 μm thick) were deparaffinized in two changes of 100% xylene for 5 min each and then hydrated in two changes of 100% ethanol for 5 min each and 90 and 70% ethanol for 1 min each. For antigen retrieval, UNI-TRIEVE (universal mild temperature retrieval solution) was used to incubate the slides at 60°C for 30 min. Afterward, slides were rinsed in phosphate-buffered saline (PBS) and blocked with normal horse serum for 30 min. Serum was removed, and sections were incubated with primary antibody at appropriate dilution (1:200) in normal horse serum overnight at 4°C. Sections were rinsed in PBS with 0.05% Tween 20 (PBS-T) and then incubated with secondary antibody at an appropriate concentration (1:400) for ~30 min in the dark and then rinsed three times in PBS-T for 5 min before mounting with a DAPI-containing medium (VECTASHIELD Antifade Mounting Medium with DAPI, cat. number H-1200, Vector), which counterstains the nuclei. Primary antibodies for detection of NETs were as follows: NE antibody (G-2; sc-55549; Santa Cruz Biotechnology) and anti-histone H3 antibody (citrulline R2 + R8 + R17; ab5103, Abcam). Secondary antibodies were the following: goat anti-rabbit immunoglobulin G (IgG) heavy and light chain (H&L) Alexa Fluor 488 (ab150081, Abcam) and goat anti-mouse IgG H&L Alexa Fluor 594 (ab150116, Abcam).

An inverted widefield microscope (WF1-Zeiss) with light-emitting diode illumination Zeiss Axio Observer and the highly sensitive Hamamatsu Flash 4 camera were used for fluorescent imaging. *Z*-stack images were collected at 63× magnification. Fiji and Icy (*84*) were used for three-dimensional (3D) visualization of *Z*-stack images. Huygens software was used for deconvolution of *Z*-stack images.

ELISA for NETs

NETs in plasma were determined as NE/DNA complexes in human samples and MPO/DNA complexes in mouse samples. For the human ELISA, we used the precoated and blocked plates of the Hycult Biotech human NE ELISA (HK319-02). Undiluted plasma samples (50 μl) were incubated for 2 hours at room temperature with 350 rpm agitation and washed three times with PBS-T. The anti–DNA-POD (peroxidase) antibody (Cell Death Detection ELISA Kit, Roche) was diluted 1:100, and the plate was incubated for 2 hours at room temperature, followed by five washes with PBS-T and incubation with trimethylboron substrate. Signal was acquired at 450 nm.

For the mouse ELISA, the biotinylated primary mouse anti-MPO antibody (1 μg/ml final concentration; HM1051BT, Hycult Biotech) was coated onto a streptavidin-coated plate from the Cell Death Detection ELISA Kit (Roche) at 4°C overnight, followed by three washes with PBS-T. The plates were subsequently blocked for 2 hours with 1% bovine serum albumin (BSA) in PBS, and 50 μl of undiluted mouse serum was added to wells. The plate was incubated for 2 hours at room temperature with agitation (300 rpm on a plate shaker), followed by three washes with PBS-T and addition of 50 μl per well of anti–DNA-POD from the Roche Cell Death ELISA kit (1:100). The plate was incubated for 2 hours with agitation at room temperature, washed five times with PBST, and developed with ABTS [2,2'-azino-bis(3-ethylbenzothiazoline-6-sulfonic acid)].

ELISA kits

The following kits were used for plasma quantifications, according to the manufacturer's instructions: Cell Death Detection ELISAPLUS (11920685001, Roche), Human Interleukin 8 Quantikine ELISA (S8000C, R&D Systems), mouse G-CSF Quantikine ELISA (MCS00, R&D Systems), human G-CSF Quantikine ELISA (SCS50, R&D Systems), mouse ICAM-1 ELISA (DY796, R&D Systems), and mouse CD36 ELISA (EMCD36, Thermo Fisher Scientific).

Human neutrophil isolation and stimulation

Cells were purified by a first centrifugation of whole blood over Histopaque-1119 (Sigma) followed by a discontinuous Percoll (Sigma) gradient (*85*). All experiments were done in RPMI-1640 (without phenol red, Gibco) supplemented with 10 mM Hepes and 0.05% human serum albumin (Albutein, Grifols). For NET induction, 10^5 neutrophils were seeded onto glass coverslips in a 24-well plate and incubated with inhibitors for 30 min, followed by 15 min of priming with TNF-α and addition of the stimuli.

Luminol assay

To assess ROS production, we activated 1×10^5 neutrophils (after treatment with inhibitors/ROS scavengers) with 50 nM PMA. ROS production was measured by monitoring luminol (50 μM) luminescence in the presence of horseradish peroxidase (1.2 U/ml) (*85*).

Mice

Mouse breeding, infections, and isolation of peritoneal neutrophils were approved by the Berlin state authority Landesamt für Gesundheit und Soziales. Animals were bred at the Max Planck Institute for Infection Biology. Mice were housed in specific pathogen–free conditions, maintained on a 12-hour light/dark cycle, and fed ad libitum.

$NE^{-/-}$ (*86*), $NE/PR3^{-/-}$ (*9*), and $DNase\ 1^{-/-}$ (*87*) mice were previously described. $PAD4^{-/-}$ mice (*88*) were a gift from D. Wagner.

Mouse neutrophil isolation and stimulation

Murine neutrophils were isolated from peritoneal cavities after elicitation with casein (Sigma) and centrifugation over Percoll as previously described (*89*). Cells were seeded onto glass coverslips at 10^5 per well in 24-well plates in RPMI (Gibco) containing penicillin-streptomycin (Gibco), glutamine (Gibco), 1% murine $DNase\ 1^{-/-}$ serum, and murine G-CSF (100 ng/ml; PeproTech). After 30 min of equilibration and 15 min of TNF-α priming, cells were stimulated with 100 nM PMA, or 20 μM heme. NETs were quantified after 15 hours of stimulation, as described below.

Quantification of NET formation

The quantification of NETosis was carried out as previously described (*90*). Briefly, cells were fixed for 30 min at room temperature in 2% paraformaldehyde, permeabilized with 0.5% Triton X-100, and blocked for 30 min in blocking buffer. Cells were then stained with the anti-NE antibody (1:200; 481001, Calbiochem) and an antibody directed against the nucleosomal complex of histone 2A, histone 2B, and chromatin (PL2-3; 1 μg/ml) (*91*), as well as the secondary antibodies

goat anti-mouse IgG Alexa Fluor 568 (1:500), goat anti-rabbit IgG Alexa Fluor 488 (1:500), and Hoechst 33342 (Sigma-Aldrich). Samples were mounted on coverslips with Mowiol. Image acquisition was done using a Leica DMR upright fluorescence microscope equipped with a JENOPTIK B/W digital microscope camera and analyzed using ImageJ/Fiji software.

Heme preparation

Heme for in vitro stimulation of neutrophils and for standard curve was prepared fresh on the day of the experiment. A 10 mM stock solution was prepared by dissolving 0.0325 g of hemin (H651-9, Frontier Scientific) in 5 ml of dimethyl sulfoxide. An intermediate 1:10 dilution in PBS was made before stimulating the cells.

Quantification of plasma heme

Heme was quantified using the formic acid assay (*92*). Briefly, samples were diluted 1:50 in H_2O in white 96-well plates. The heme concentration was determined after the addition of 100% formic acid (150 µl per well, Merck) to all samples and absorbance measurement at 405 nm using a microplate reader. Measurements were compared with a hemin standard curve in the range of 0.25 to 16 µM in H_2O.

P. falciparum culture

P. falciparum parasites were cultured using standard procedures as described previously (*93*). Parasites were grown at 5% hematocrit in RPMI 1640 medium, 0.5% AlbuMAX II (Invitrogen), 0.25% sodium bicarbonate, and gentamicin (0.1 mg/ml). Cultures were incubated at 37°C in an atmosphere of 5% oxygen, 5% carbon dioxide, and 90% nitrogen.

Trophozoite and merozoite preparation

A late-stage *P. falciparum* culture was washed and taken up in 2 ml of RPMI and layered onto 5 ml of a 60% Percoll solution. The mixture was centrifuged at 2000*g* for 20 min at 20°C, and trophozoites were collected at the interphase between RPMI and Percoll, whereas uninfected RBCs and ring stage iRBCs were pelleted. Parasites were washed three times with RPMI and iRBCs were pelleted. For merozoite isolation, iRBCs were lysed with 0.03% saponin solution. Subsequently, the sample was washed three times with PBS and taken up in RPMI. The concentration of merozoites was determined by use of a Neubauer chamber.

Isolation of DVs from *P. falciparum*

Late trophozoite cultures with 10% parasitemia were allowed to complete schizogony and reinfection. Cultures were stratified on a discontinuous Percoll-mannitol gradient, and expelled DVs were collected on the 10/40% Percoll interphase as previously described (*94*). The collected interphase was passed through a 27-gauge needle and separated by density using 42% Percoll. The intact DVs could be collected as dark gray–colored bottom fraction. DVs were resuspended in uptake buffer [2 mM $MgSO_4$ (pH 7.4), 100 mM KCl, 25 mM Hepes, 25 mM $NaHCO_3$, and 5 mM Na_3PO_4], washed, and used in subsequent experiments.

P. chabaudi infections, plasma, and tissue preparation

Male mice aged 8 to 15 weeks were infected by intravenous injection of viable *P. chabaudi* AS parasites (WT) or PccASluc [luciferase-expressing; (*45*)]. Male mice were used because they demonstrate higher parasitemia than females. To ensure viability of the parasites, we thawed a frozen aliquot and injected it intraperitoneally into a transfer mouse. The number of asexual parasites intravenously injected into each mouse was adjusted according to body weight so that each animal received 1×10^4 iRBCs per 20 g. Parasitemia was monitored from day 5 after infection every 48 hours by Giemsa-stained thin blood smear. Anti–G-CSF antibody (150 µl per mouse, R&D Systems) or isotype control (150 µl per mouse, R&D Systems) was injected intravenously on day 7 after infection.

Mice were bled by cardiac puncture under nonrecovery deep anesthesia. Blood was kept from coagulating by addition of 50 µM final concentration of EDTA (Sigma). Plasma was generated by centrifugation at 10,000*g* at 4°C for 10 min. Plasma was aliquoted, snap-frozen in liquid nitrogen, and stored at −80°C until further use. Plasma was always thawed on ice.

Organs were harvested without additional perfusion (except in parasite sequestration experiments), as blood was removed by terminal bleeding of the animals. The organs were fixed for 20 hours at room temperature in 2% paraformaldehyde.

Immunohistochemistry

The blinded scoring of liver pathology and the counting of parasites sequestered in the microvasculature of the livers were performed by trained pathologists at the iPATH.Berlin Core Unit for immunopathology of experimental model organisms from H&E-stained paraffin sections of 1-µm thickness. The scores are defined in Table 1.

Acute lung injury

The score sheet shown in Table 2 was modified from (*96*). Animals were assigned to individual categories matching their histopathological signs.

Immunofluorescence of mouse tissue sections

Mouse tissues were fixed in 2% paraformaldehyde solution in tris-buffered saline (pH 7.4) for 20 hours at room temperature. The tissue was then dehydrated and paraffin-embedded (60°C) using a Leica TP1020 tissue processor. Paraffin blocks were cut to 3 µm, and sections were mounted and dried on Superfrost Plus slides (Thermo Scientific) avoiding temperatures above 37°C. After dewaxing and rehydration, sections were incubated in heat-induced epitope retrieval (HIER) buffer (pH 6; citrate buffer) (20 min at 96°C in a steam cooker; Braun). After antigen retrieval, sections were left in the respective HIER buffer at room temperature to cool below 30°C, rinsed three times with deionized water and once with PBS (pH 7.4), and permeabilized for 5 min with 0.5% Triton X-100 in PBS at room temperature, followed by three rinsing steps with PBS.

Sections were surrounded with peroxidase-antiperoxidase pen and treated with blocking buffer for 30 min to prevent nonspecific binding. Primary antibodies were diluted in blocking buffer and incubated on the sections overnight at room temperature. The following primary antibodies were used for tissue sections: anti-mouse ICAM (dilution 1:200; AF796, Novus Biologicals), anti-mouse calgranulin A [dilution 1:50; in-house (*5*), Max Planck Institute for Infection Biology], and anti-CD36 (dilution 1:200; NB400-144, Novus). We used secondary antibodies raised in donkey and preabsorbed against serum proteins from multiple host species (Jackson ImmunoResearch). Dilution and blocking were done in PBS supplemented with 1% BSA, 2% normal donkey serum, 5% cold water fish gelatin, 0.05% Tween 20, and 0.05% Triton X-100.

Slides were mounted using Mowiol and digitized with a ZEISS Axio Scan.Z1. This is an automated microscope that generates a series of overlapping photographs that are assembled into a single image of a complete organ section in an operator-independent manner. The relative abundance of calgranulin A (neutrophils), ICAM-1, or CD36 was then calculated by normalizing the respective pixels to the DAPI pixels (total tissue area), using the software package Volocity 6.3.

Determination of liver enzyme concentration in mouse plasma

The concentration of the hepatocyte-specific enzyme AST in the plasma of experimental animals was determined by the routine veterinarian service laboratory at SYNLAB.vet GmbH (Berlin, Germany).

FACS analysis of mouse whole blood

Mouse whole blood (100 µl) was stained directly by the addition of 100 µl of fluorescence-activated cell sorting (FACS) antibodies diluted 1:100 in FACS buffer (PBS supplemented with 2.5% fetal calf serum and 0.1% NaN_3) for 30 min. Cells were treated with 3 ml of 1-step Fix/Lyse (00-5333-54, eBioscience) for 60 min at room temperature, washed once as per the manufacturer's instructions, and taken up in 250 µl of FACS buffer before analysis using a MACSQuant Analyzer. Antibodies were all from BD Biosciences: V500 anti-CD45 (561487), fluorescein isothiocyanate anti-CD3 (561798), phycoerythrin (PE) anti-CD115 (565249), and PerCP-Cy5.5 anti-Ly6G/C (561103). Neutrophils were defined as $CD45^+$ $CD115^-$ $Ly6G/C^+$ cells.

Assessment of sequestration of luciferase-expressing parasites

Mice were infected with a luciferase-expressing strain of *P. chabaudi* [PccASluc (*45*)] as described above but kept on a reverse light cycle, as sequestration occurs during the dark cycle (*45*). At the time of maximum sequestration (1200–1400 hours coordinated universal time, reverse light), mice were euthanized and perfused systemically by injection of 10 ml of PBS into the heart. Organs were harvested, and 0.1 g of tissue was transferred to a Precellys homogenizer tube in PBS and dissociated for one cycle, 10 s at 4500 rpm in a Precellys Evolution Homogenizer. The sample was then diluted 1:10 in PBS, and an equal volume (100 µl) of Bright-Glo substrate (Promega) was added. Luciferase activity was measured after 2 min of incubation using a PerkinElmer VICTOR X Light Multilabel Plate Reader.

Injection of exogenous NETs and control chromatin

Murine NETs were prepared from WT peritoneal neutrophils with PMA as described above, washed three times with PBS to remove residual PMA, scraped from the plate, and sonicated for 15 s at 70% power using a Bandelin SONOPULS sonicator. DNA concentration was quantified by PicoGreen assay (P11496, Thermo Fisher Scientific) or NanoDrop measurements. For removal of DNA, the sample was then treated with 2 U of DNase 1 from the TURBO DNA-free Kit (AM1907, Thermo Fisher Scientific) overnight at 37°C. The kit was chosen because it contains a DNase-inactivating agent, which was used according to the manufacturer's specifications to ensure that no DNase activity was introduced into injected mice. Complete digestion of DNA was confirmed by both agarose gel electrophoresis and PicoGreen measurement. Mice were injected with an amount of NETs or chromatin that was previously observed to have accumulated in infected WT mice (300 ng/ml of blood). We assumed a blood volume of an adult male mouse of 1.5 ml and therefore injected 450 ng of either NETs or chromatin into each mouse.

Control chromatin was isolated from bone marrow–derived macrophages, which were prepared according to standard protocol (*96*). Chromatin was prepared as previously described (*97*). Briefly, when cells were confluent, they were harvested, washed, and counted. Three hundred microliters of hypotonic buffer A [10 mM Hepes (pH 7.5), 10 mM KCl, 3 mM NaCl, 3 mM $MgCl_2$, 1 mM EDTA, 1 mM EGTA, and 2 mM dithiothreitol and a general protease inhibitor cocktail (78430, Thermo Fisher Scientific)] was added per 5×10^6 cells and incubated on ice for 15 min. Subsequently, 0.05 volumes of 10% Nonidet P-40 was added, and the cells were vortexed and centrifuged at 500*g* for 10 min at 4°C. The supernatant was discarded, and the nuclei in the pellet were washed in buffer A and subsequently resuspended in 50 µl of ice-cold buffer NE [20 mM Hepes (pH 7.5), 25% glycerol, 0.8 mM KCl, 1 mM $MgCl_2$, 1% Nonidet P-40, 0.5 mM EDTA, and 2 mM dithiothreitol]. After 20 min of incubation on ice with occasional mixing, the samples were centrifuged at 14,000*g* for 15 min at 4°C. The supernatant was discarded, and the pellet containing the chromatin was resuspended in double-distilled H_2O. Chromatin concentration was determined by PicoGreen assay (see above), and samples were stored at −80°C.

Macrophage stimulation with NETs

Monocytes were isolated by magnetic $CD14^+$ selection (130-050-201, Miltenyi Biotec) and differentiated for 7 days into macrophages in RPMI 1640 containing penicillin-streptomycin, glutamine, and human macrophage CSF (5 ng/ml). On the day of the experiment, 3×10^6 neutrophils were stimulated for 4 hours with 50 nM PMA. The resulting NETs were washed three times with PBS, harvested by scraping, and sonicated. The NET concentration was determined by PicoGreen assay. Macrophages were stimulated for 12 hours with isolated NETs (1 µg/ml), hemozoin (100 µg/ml; Sigma), TNF-α (2 ng/ml; PeproTech), or LPS from *Salmonella* (100 ng/ml; Enzo Life Sciences).

SUPPLEMENTARY MATERIALS

immunology.sciencemag.org/cgi/content/full/4/40/eaaw0336/DC1

Fig. S1. In vitro stimulations of human neutrophils.
Fig. S2. Necrosis and sequestration in the livers of *P. chabaudi*–infected mice.
Fig. S3. Pathology in the lungs of *P. chabaudi*–infected animals.
Fig. S4. Parasitemia of NET fragment–injected mice.
Fig. S5. Immunofluorescence images used to quantify neutrophils in livers of infected mice.
Fig. S6. Quantification of free circulating heme in plasma of uninfected and infected animals, treated with a G-CSF neutralizing antibody or isotype control antibody.
Table S1. Patient information of cohort 1 and 2 in Gabon.
Table S2. Clinical characteristics of the patient population in Mozambique.
Table S3. Clinical diagnosis and classification of subjects whose ocular tissue was used for immunofluorescence experiments.
Data file S1. Raw data in Excel spreadsheet.
View/request a protocol for this paper from *Bio-protocol*.

REFERENCES AND NOTES

1. B. Amulic, C. Cazalet, G. L. Hayes, K. D. Metzler, A. Zychlinsky, Neutrophil function: From mechanisms to disease. *Annu. Rev. Immunol.* **30**, 459–489 (2012).
2. V. Brinkmann, U. Reichard, C. Goosmann, B. Fauler, Y. Uhlemann, D. S. Weiss, Y. Weinrauch, A. Zychlinsky, Neutrophil extracellular traps kill bacteria. *Science* **303**, 1532–1535 (2004).
3. V. Papayannopoulos, Neutrophil extracellular traps in immunity and disease. *Nat. Rev. Immunol.* **18**, 134–147 (2018).
4. A. Hakkim, B. G. Furnrohr, K. Amann, B. Laube, U. A. Abed, V. Brinkmann, M. Herrmann, R. E. Voll, A. Zychlinsky, Impairment of neutrophil extracellular trap degradation is associated with lupus nephritis. *Proc. Natl. Acad. Sci. U.S.A.* **107**, 9813–9818 (2010).

5. B. Amulic, S. L. Knackstedt, U. Abu Abed, N. Deigendesch, C. J. Harbort, B. E. Caffrey, V. Brinkmann, F. L. Heppner, P. W. Hinds, A. Zychlinsky, Cell-cycle proteins control production of neutrophil extracellular traps. *Dev. Cell* **43**, 449–462.e5 (2017).
6. A. Hakkim, T. A. Fuchs, N. E. Martinez, S. Hess, H. Prinz, A. Zychlinsky, H. Waldmann, Activation of the Raf-MEK-ERK pathway is required for neutrophil extracellular trap formation. *Nat. Chem. Biol.* **7**, 75–77 (2011).
7. T. A. Fuchs, U. Abed, C. Goosmann, R. Hurwitz, I. Schulze, V. Wahn, Y. Weinrauch, V. Brinkmann, A. Zychlinsky, Novel cell death program leads to neutrophil extracellular traps. *J. Cell Biol.* **176**, 231–241 (2007).
8. V. Papayannopoulos, K. D. Metzler, A. Hakkim, A. Zychlinsky, Neutrophil elastase and myeloperoxidase regulate the formation of neutrophil extracellular traps. *J. Cell Biol.* **191**, 677–691 (2010).
9. A. Warnatsch, M. Ioannou, Q. Wang, V. Papayannopoulos, Inflammation. Neutrophil extracellular traps license macrophages for cytokine production in atherosclerosis. *Science* **349**, 316–320 (2015).
10. G. Sollberger, A. Choidas, G. L. Burn, P. Habenberger, R. Di Lucrezia, S. Kordes, S. Menninger, J. Eickhoff, P. Nussbaumer, B. Klebl, R. Krüger, A. Herzig, A. Zychlinsky, Gasdermin D plays a vital role in the generation of neutrophil extracellular traps. *Sci. Immunol.* **3**, eaar6689 (2018).
11. K. Kessenbrock, L. Fröhlich, M. Sixt, T. Lämmermann, H. Pfister, A. Bateman, A. Belaaouaj, J. Ring, M. Ollert, R. Fässler, D. E. Jenne, Proteinase 3 and neutrophil elastase enhance inflammation in mice by inactivating antiinflammatory progranulin. *J. Clin. Invest.* **118**, 2438–2447 (2008).
12. A. Thanabalasuriar, B. N. V. Scott, M. Peiseler, M. E. Willson, Z. Zeng, P. Warrener, A. E. Keller, B. G. J. Surewaard, E. A. Dozier, J. T. Korhonen, L. I. T. Cheng, M. Gadjeva, C. K. Stover, A. DiGiandomenico, P. Kubes, Neutrophil extracellular traps confine *Pseudomonas aeruginosa* ocular biofilms and restrict brain invasion. *Cell Host Microbe* **25**, 526–536.e4 (2019).
13. C. K. Smith, M. J. Kaplan, The role of neutrophils in the pathogenesis of systemic lupus erythematosus. *Curr. Opin. Rheumatol.* **27**, 448–453 (2015).
14. C. Silvestre-Roig, Q. Braster, K. Wichapong, E. Y. Lee, J. M. Teulon, N. Berrebeh, J. Winter, J. M. Adrover, G. S. Santos, A. Froese, P. Lemnitzer, A. Ortega-Gómez, R. Chevre, J. Marschner, A. Schumski, C. Winter, L. Perez-Olivares, C. Pan, N. Paulin, T. Schoufour, H. Hartwig, S. González-Ramos, F. Kamp, R. T. A. Megens, K. A. Mowen, M. Gunzer, L. Maegdefessel, T. Hackeng, E. Lutgens, M. Daemen, J. von Blume, H. J. Anders, V. O. Nikolaev, J. L. Pellequer, C. Weber, A. Hidalgo, G. A. F. Nicolaes, G. C. L. Wong, O. Soehnlein, Externalized histone H4 orchestrates chronic inflammation by inducing lytic cell death. *Nature* **569**, 236–240 (2019).
15. A. Schreiber, A. Rousselle, J. U. Becker, A. von Mässenhausen, A. Linkermann, R. Kettritz, Necroptosis controls NET generation and mediates complement activation, endothelial damage, and autoimmune vasculitis. *Proc. Natl. Acad. Sci. U.S.A.* **114**, E9618–E9625 (2017).
16. K. Martinod, D. D. Wagner, Thrombosis: Tangled up in NETs. *Blood* **123**, 2768–2776 (2014).
17. C. M. Feintuch, A. Saidi, K. Seydel, G. Chen, A. Goldman-Yassen, N. K. Mita-Mendoza, R. S. Kim, P. S. Frenette, T. Taylor, J. P. Daily, Activated neutrophils are associated with pediatric cerebral malaria vasculopathy in Malawian children. *MBio* **7**, e01300–15 (2016).
18. H. J. Lee, A. Georgiadou, M. Walther, D. Nwakanma, L. B. Stewart, M. Levin, T. D. Otto, D. J. Conway, L. J. Coin, A. J. Cunnington, Integrated pathogen load and dual transcriptome analysis of systemic host-pathogen interactions in severe malaria. *Sci. Transl. Med.* **10**, eaar3619 (2018).
19. T. A. Ghebreyesus, K. Admasu, Countries must steer new response to turn the malaria tide. *Lancet* **392**, 2246–2247 (2018).
20. L. H. Miller, H. C. Ackerman, X.-z. Su, T. E. Wellems, Malaria biology and disease pathogenesis: Insights for new treatments. *Nat. Med.* **19**, 156–167 (2013).
21. K. Deroost, T.-T. Pham, G. Opdenakker, P. E. van den Steen, The immunological balance between host and parasite in malaria. *FEMS Microbiol. Rev.* **40**, 208–257 (2016).
22. K. W. Deitsch, R. Dzikowski, Variant gene expression and antigenic variation by malaria parasites. *Annu. Rev. Microbiol.* **71**, 625–641 (2017).
23. S. C. Wassmer, G. E. R. Grau, Severe malaria: What's new on the pathogenesis front? *Int. J. Parasitol.* **47**, 145–152 (2017).
24. G. E. R. Grau, A. G. Craig, Cerebral malaria pathogenesis: Revisiting parasite and host contributions. *Future Microbiol.* **7**, 291–302 (2012).
25. R. T. Gazzinelli, P. Kalantari, K. A. Fitzgerald, D. T. Golenbock, Innate sensing of malaria parasites. *Nat. Rev. Immunol.* **14**, 744–757 (2014).
26. A. J. Cunnington, M. Njie, S. Correa, E. N. Takem, E. M. Riley, M. Walther, Prolonged neutrophil dysfunction after *Plasmodium falciparum* malaria is related to hemolysis and heme oxygenase-1 induction. *J. Immunol.* **189**, 5336–5346 (2012).
27. S. Boström, C. Schmiegelow, U. Abu Abed, D. T. R. Minja, J. Lusingu, V. Brinkmann, Y. J. Honkpehedji, M. M. Loembe, A. A. Adegnika, B. Mordmüller, M. Troye-Blomberg, B. Amulic, Neutrophil alterations in pregnancy-associated malaria and induction of neutrophil chemotaxis *byPlasmodium falciparum*. *Parasite Immunol.* **39**, e12433 (2017).
28. B. C. Rocha, P. E. Marques, F. M. de Souza Leoratti, C. Junqueira, D. B. Pereira, L. Ribeiro do Valle Antonelli, G. B. Menezes, D. T. Golenbock, R. T. Gazzinelli, Type I interferon transcriptional signature in neutrophils and low-density granulocytes are associated with tissue damage in malaria. *Cell Rep.* **13**, 2829–2841 (2015).
29. J.-W. Lin, J. Sodenkamp, D. Cunningham, K. Deroost, T. C. Tshitenge, S. McLaughlin, T. J. Lamb, B. Spencer-Dene, C. Hosking, J. Ramesar, C. J. Janse, C. Graham, A. O'Garra, J. Langhorne, Signatures of malaria-associated pathology revealed by high-resolution whole-blood transcriptomics in a rodent model of malaria. *Sci. Rep.* **7**, 41722 (2017).
30. L. Chen, Z.-H. Zhang, F. Sendo, Neutrophils play a critical role in the pathogenesis of experimental cerebral malaria. *Clin. Exp. Immunol.* **120**, 125–133 (2000).
31. M. K. Sercundes, L. S. Ortolan, D. Debone, P. V. Soeiro-Pereira, E. Gomes, E. H. Aitken, A. C. Neto, M. Russo, M. R. D' Império Lima, J. M. Alvarez, S. Portugal, C. R. F. Marinho, S. Epiphanio, Targeting neutrophils to prevent malaria-associated acute lung Injury/ acute respiratory distress syndrome in mice. *PLOS Pathog.* **12**, e1006054 (2016).
32. M. R. Gillrie, K. Lee, D. C. Gowda, S. P. Davis, M. Monestier, L. Cui, T. T. Hien, N. P. J. Day, M. Ho, *Plasmodium falciparum* histones induce endothelial proinflammatory response and barrier dysfunction. *Am. J. Pathol.* **180**, 1028–1039 (2012).
33. V. S. Baker, G. E. Imade, N. B. Molta, P. Tawde, S. D. Pam, M. O. Obadofin, S. A. Sagay, D. Z. Egah, D. Iya, B. B. Afolabi, M. Baker, K. Ford, R. Ford, K. H. Roux, T. C. S. Keller III, Cytokine-associated neutrophil extracellular traps and antinuclear antibodies in *Plasmodium falciparum* infected children under six years of age. *Malar. J.* **7**, 41 (2008).
34. S. Kho, G. Minigo, B. Andries, L. Leonardo, P. Prayoga, J. R. Poespoprodjo, E. Kenangalem, R. N. Price, T. Woodberry, N. M. Anstey, T. W. Yeo, Circulating neutrophil extracellular traps and neutrophil activation are increased in proportion to disease severity in human malaria. *J. Infect. Dis.* **219**, 1994–2004 (2018).
35. J. F. T. Kun, R. J. Schmidt-Ott, L. G. Lehman, B. Lell, D. Luckner, B. Greve, P. Matousek, P. G. Kremsner, Merozoite surface antigen 1 and 2 genotypes and rosetting of *Plasmodium falciparum* in severe and mild malaria in Lambaréné, Gabon. *Trans. R. Soc. Trop. Med. Hyg.* **92**, 110–114 (1998).
36. WHO, Guidelines for the treatment of malaria. Third Edition (2015); http://www.who.int/malaria/publications/atoz/9789241549127/en.
37. T. E. Taylor, W. J. Fu, R. A. Carr, R. O. Whitten, J. G. Mueller, N. G. Fosiko, S. Lewallen, N. G. Liomba, M. E. Molyneux, Differentiating the pathologies of cerebral malaria by *postmortem* parasite counts. *Nat. Med.* **10**, 143–145 (2004).
38. V. Barrera, I. J. C. MacCormick, G. Czanner, P. S. Hiscott, V. A. White, A. G. Craig, N. A. V. Beare, L. H. Culshaw, Y. Zheng, S. C. Biddolph, D. A. Milner, S. Kamiza, M. E. Molyneux, T. E. Taylor, S. P. Harding, Neurovascular sequestration in paediatric *P. falciparum* malaria is visible clinically in the retina. *eLife* **7**, e32208 (2018).
39. I. J. C. MacCormick, N. A. V. Beare, T. E. Taylor, V. Barrera, V. A. White, P. Hiscott, M. E. Molyneux, B. Dhillon, S. P. Harding, Cerebral malaria in children: Using the retina to study the brain. *Brain* **137** (Pt. 8), 2119–2142 (2014).
40. G. Chen, D. Zhang, T. A. Fuchs, D. Manwani, D. D. Wagner, P. S. Frenette, Heme-induced neutrophil extracellular traps contribute to the pathogenesis of sickle cell disease. *Blood* **123**, 3818–3827 (2014).
41. E. F. Kenny, A. Herzig, R. Krüger, A. Muth, S. Mondal, P. R. Thompson, V. Brinkmann, H. von Bernuth, A. Zychlinsky, Diverse stimuli engage different neutrophil extracellular trap pathways. *eLife* **6**, e24437 (2017).
42. I. Neeli, M. Radic, Opposition between PKC isoforms regulates histone deimination and neutrophil extracellular chromatin release. *Front. Immunol.* **4**, 38 (2013).
43. K. Martinod, M. Demers, T. A. Fuchs, S. L. Wong, A. Brill, M. Gallant, J. Hu, Y. Wang, D. D. Wagner, Neutrophil histone modification by peptidylarginine deiminase 4 is critical for deep vein thrombosis in mice. *Proc. Natl. Acad. Sci. U.S.A.* **110**, 8674–8679 (2013).
44. G. Sollberger, B. Amulic, A. Zychlinsky, Neutrophil extracellular trap formation is independent of de novo gene expression. *PLOS ONE* **11**, e0157454 (2016).
45. T. Brugat, D. Cunningham, J. Sodenkamp, S. Coomes, M. Wilson, P. J. Spence, W. Jarra, J. Thompson, C. Scudamore, J. Langhorne, Sequestration and histopathology in *Plasmodium chabaudi* malaria are influenced by the immune response in an organ-specific manner. *Cell. Microbiol.* **16**, 687–700 (2014).
46. K. Deroost, N. Lays, T.-T. Pham, D. Baci, K. van den Eynde, M. Komuta, M. Prato, T. Roskams, E. Schwarzer, G. Opdenakker, P. E. van den Steen, Hemozoin induces hepatic inflammation in mice and is differentially associated with liver pathology depending on the *Plasmodium* strain. *PLOS ONE* **9**, e113519 (2014).
47. G. S. Garcia-Romo, S. Caielli, B. Vega, J. Connolly, F. Allantaz, Z. Xu, M. Punaro, J. Baisch, C. Guiducci, R. L. Coffman, F. J. Barrat, J. Banchereau, V. Pascual, Netting neutrophils are major inducers of type I IFN production in pediatric systemic lupus erythematosus. *Sci. Transl. Med.* **3**, 73ra20 (2011).
48. G. Marsman, S. Zeerleder, B. M. Luken, Extracellular histones, cell-free DNA, or nucleosomes: Differences in immunostimulation. *Cell Death Dis.* **7**, e2518 (2016).
49. R. N. Maina, D. Walsh, C. Gaddy, G. Hongo, J. Waitumbi, L. Otieno, D. Jones, B. R. Ogutu, Impact of *Plasmodium falciparum* infection on haematological parameters in children living in Western Kenya. *Malar. J.* **9** (suppl. 3), S4 (2010).

50. P. Olliaro, A. Djimdé, G. Dorsey, C. Karema, A. Mårtensson, J.-L. Ndiaye, S. B. Sirima, M. Vaillant, J. Zwang, Hematologic parameters in pediatric uncomplicated *Plasmodium falciparum* malaria in sub-Saharan Africa. *Am. J. Trop. Med. Hyg.* **85**, 619–625 (2011).
51. M. Kotepui, D. Piwkham, B. PhunPhuech, N. Phiwklam, C. Chupeerach, S. Duangmano, Effects of malaria parasite density on blood cell parameters. *PLOS ONE* **10**, e0121057 (2015).
52. O. Soehnlein, S. Steffens, A. Hidalgo, C. Weber, Neutrophils as protagonists and targets in chronic inflammation. *Nat. Rev. Immunol.* **17**, 248–261 (2017).
53. L. Yang, R. M. Froio, T. E. Sciuto, A. M. Dvorak, R. Alon, F. W. Luscinskas, ICAM-1 regulates neutrophil adhesion and transcellular migration of TNF-α-activated vascular endothelium under flow. *Blood* **106**, 584–592 (2005).
54. D. A. Cunningham, J.-W. Lin, T. Brugat, W. Jarra, I. Tumwine, G. Kushinga, J. Ramesar, B. Franke-Fayard, J. Langhorne, ICAM-1 is a key receptor mediating cytoadherence and pathology in the *Plasmodium chabaudi* malaria model. *Malar. J.* **16**, 185 (2017).
55. J. D. Smith, A. G. Craig, N. Kriek, D. Hudson-Taylor, S. Kyes, T. Fagan, R. Pinches, D. I. Baruch, C. I. Newbold, L. H. Miller, Identification of a *Plasmodium falciparum* intercellular adhesion molecule-1 binding domain: A parasite adhesion trait implicated in cerebral malaria. *Proc. Natl. Acad. Sci. U.S.A.* **97**, 1766–1771 (2000).
56. A. Cabrera, D. Neculai, K. C. Kain, CD36 and malaria: Friends or foes? A decade of data provides some answers. *Trends Parasitol.* **30**, 436–444 (2014).
57. B. Stoiser, S. Looareesuwan, F. Thalhammer, F. Daxböck, S. Chullawichit, I. El-Menyawi, W. Graninger, H. Burgmann, Serum concentrations of granulocyte-colony stimulating factor in complicated *Plasmodium falciparum* malaria. *Eur. Cytokine Netw.* **11**, 75–80 (2000).
58. E. H. Aitken, A. Alemu, S. J. Rogerson, Neutrophils and malaria. *Front. Immunol.* **9**, 3005 (2018).
59. A. V. Graça-Souza, M. A. B. Arruda, M. S. de Freitas, C. Barja-Fidalgo, P. L. Oliveira, Neutrophil activation by heme: Implications for inflammatory processes. *Blood* **99**, 4160–4165 (2002).
60. F. F. Dutra, M. T. Bozza, Heme on innate immunity and inflammation. *Front. Pharmacol.* **5**, 115 (2014).
61. R. N. Rodrigues-da-Silva, J. da Costa Lima-Junior, B. de Paula Fonseca e Fonseca, P. R. Z. Antas, A. Baldez, F. L. Storer, F. Santos, D. M. Banic, J. de Oliveira-Ferreira, Alterations in cytokines and haematological parameters during the acute and convalescent phases of *Plasmodium falciparum* and *Plasmodium vivax* infections. *Mem. Inst. Oswaldo Cruz* **109**, 154–162 (2014).
62. S. Ladhani, B. Lowe, A. O. Cole, K. Kowuondo, C. R. J. C. Newton, Changes in white blood cells and platelets in children with falciparum malaria: Relationship to disease outcome. *Br. J. Haematol.* **119**, 839–847 (2002).
63. A. Tobon-Castano, E. Mesa-Echeverry, A. F. Miranda-Arboleda, Leukogram profile and clinical status in *vivax* and *falciparum* malaria patients from Colombia. *J. Trop. Med.* **2015**, 796182 (2015).
64. D. S. Squire, R. H. Asmah, C. A. Brown, D. N. Adjei, N. Obeng-Nkrumah, P. F. Ayeh-Kumi, Effect of *Plasmodium falciparum* malaria parasites on haematological parameters in Ghanaian children. *J. Parasit. Dis.* **40**, 303–311 (2016).
65. G. D. H. Turner, H. Morrison, M. Jones, T. M. E. Davis, S. Looareesuwan, I. D. Buley, K. C. Gatter, C. I. Newbold, S. Pukritayakamee, B. Nagachinta, N. J. White, A. R. Berendt, An immunohistochemical study of the pathology of fatal malaria. Evidence for widespread endothelial activation and a potential role for intercellular adhesion molecule-1 in cerebral sequestration. *Am. J. Pathol.* **145**, 1057–1069 (1994).
66. S. K. Tessema, D. Utama, O. Chesnokov, A. N. Hodder, C. S. Lin, G. L. A. Harrison, J. S. Jespersen, B. Petersen, L. Tavul, P. Siba, D. Kwiatkowski, T. Lavstsen, D. S. Hansen, A. V. Oleinikov, I. Mueller, A. E. Barry, Antibodies to intercellular adhesion molecule 1-binding *Plasmodium falciparum* erythrocyte membrane protein 1-DBLβ are biomarkers of protective immunity to malaria in a cohort of young children from Papua New Guinea. *Infect. Immun.* **86**, e00485-17 (2018).
67. A. V. Oleinikov, V. V. Voronkova, I. T. Frye, E. Amos, R. Morrison, M. Fried, P. E. Duffy, A plasma survey using 38 PfEMP1 domains reveals frequent recognition of the *Plasmodium falciparum* antigen VAR2CSA among young Tanzanian children. *PLOS ONE* **7**, e31011 (2012).
68. W. R. J. Taylor, J. Hanson, G. D. H. Turner, N. J. White, A. M. Dondorp, Respiratory manifestations of malaria. *Chest* **142**, 492–505 (2012).
69. E. Kolaczkowska, C. N. Jenne, B. G. J. Surewaard, A. Thanabalasuriar, W.-Y. Lee, M. J. Sanz, K. Mowen, G. Opdenakker, P. Kubes, Molecular mechanisms of NET formation and degradation revealed by intravital imaging in the liver vasculature. *Nat. Commun.* **6**, 6673 (2015).
70. K. Tanaka, Y. Koike, T. Shimura, M. Okigami, S. Ide, Y. Toiyama, Y. Okugawa, Y. Inoue, T. Araki, K. Uchida, Y. Mohri, A. Mizoguchi, M. Kusunoki, In vivo characterization of neutrophil extracellular traps in various organs of a murine sepsis model. *PLOS ONE* **9**, e111888 (2014).
71. W. Meng, A. Paunel-Görgülü, S. Flohé, A. Hoffmann, I. Witte, C. MacKenzie, S. E. Baldus, J. Windolf, T. T. Lögters, Depletion of neutrophil extracellular traps in vivo results in hypersusceptibility to polymicrobial sepsis in mice. *Crit. Care* **16**, R137 (2012).
72. M. Jimenez-Alcazar, C. Rangaswamy, R. Panda, J. Bitterling, Y. J. Simsek, A. T. Long, R. Bilyy, V. Krenn, C. Renné, T. Renné, S. Kluge, U. Panzer, R. Mizuta, H. G. Mannherz, D. Kitamura, M. Herrmann, M. Napirei, T. A. Fuchs, Host DNases prevent vascular occlusion by neutrophil extracellular traps. *Science* **358**, 1202–1206 (2017).
73. T. A. Fuchs, A. Brill, D. Duerschmied, D. Schatzberg, M. Monestier, D. D. Myers Jr., S. K. Wrobleski, T. W. Wakefield, J. H. Hartwig, D. D. Wagner, Extracellular DNA traps promote thrombosis. *Proc. Natl. Acad. Sci. U.S.A.* **107**, 15880–15885 (2010).
74. J. Albrengues, M. A. Shields, D. Ng, C. G. Park, A. Ambrico, M. E. Poindexter, P. Upadhyay, D. L. Uyeminami, A. Pommier, V. Küttner, E. Bružas, L. Maiorino, C. Bautista, E. M. Carmona, P. A. Gimotty, D. T. Fearon, K. Chang, S. K. Lyons, K. E. Pinkerton, L. C. Trotman, M. S. Goldberg, J. T.-H. Yeh, M. Egeblad, Neutrophil extracellular traps produced during inflammation awaken dormant cancer cells in mice. *Science* **361**, eaao4227 (2018).
75. D. Yang, Z. Han, J. J. Oppenheim, Alarmins and immunity. *Immunol. Rev.* **280**, 41–56 (2017).
76. C. H. Lim, S. S. Adav, S. K. Sze, Y. K. Choong, R. Saravanan, A. Schmidtchen, Thrombin and plasmin alter the proteome of neutrophil extracellular traps. *Front. Immunol.* **9**, 1554 (2018).
77. J. M. O'Sullivan, R. J. S. Preston, N. O'Regan, J. S. O'Donnell, Emerging roles for hemostatic dysfunction in malaria pathogenesis. *Blood* **127**, 2281–2288 (2016).
78. A. Ferreira, I. Marguti, I. Bechmann, V. Jeney, Å. Chora, N. R. Palha, S. Rebelo, A. Henri, Y. Beuzard, M. P. Soares, Sickle hemoglobin confers tolerance to *Plasmodium* infection. *Cell* **145**, 398–409 (2011).
79. C. F. Thobakgale, T. Ndung'u, Neutrophil counts in persons of African origin. *Curr. Opin. Hematol.* **21**, 50–57 (2014).
80. A. P. Reiner, G. Lettre, M. A. Nalls, S. K. Ganesh, R. Mathias, M. A. Austin, E. Dean, S. Arepalli, A. Britton, Z. Chen, D. Couper, J. D. Curb, C. B. Eaton, M. Fornage, S. F. A. Grant, T. B. Harris, D. Hernandez, N. Kamatini, B. J. Keating, M. Kubo, A. LaCroix, L. A. Lange, S. Liu, K. Lohman, Y. Meng, E. R. Mohler, S. Musani, Y. Nakamura, C. J. O'Donnell, Y. Okada, C. D. Palmer, G. J. Papanicolaou, K. V. Patel, A. B. Singleton, A. Takahashi, H. Tang, H. A. Taylor, K. Taylor, C. Thomson, L. R. Yanek, L. Yang, E. Ziv, A. B. Zonderman, A. R. Folsom, M. K. Evans, Y. Liu, D. M. Becker, B. M. Snively, J. G. Wilson, Genome-wide association study of white blood cell count in 16,388 African Americans: The continental origins and genetic epidemiology network (COGENT). *PLOS Genet.* **7**, e1002108 (2011).
81. R. E. Elphinstone, A. L. Conroy, M. Hawkes, L. Hermann, S. Namasopo, H. S. Warren, C. C. John, W. C. Liles, K. C. Kain, Alterations in systemic extracellular heme and hemopexin are associated with adverse clinical outcomes in Ugandan children with severe malaria. *J. Infect. Dis.* **214**, 1268–1275 (2016).
82. S. Ramos, A. R. Carlos, B. Sundaram, V. Jeney, A. Ribeiro, R. Gozzelino, C. Bank, E. Gjini, F. Braza, R. Martins, T. W. Ademolue, B. Blankenhaus, Z. Gouveia, P. Faísca, D. Trujillo, S. Cardoso, S. Rebelo, L. del Barrio, A. Zarjou, S. Bolisetty, A. Agarwal, M. P. Soares, Renal control of disease tolerance to malaria. *Proc. Natl. Acad. Sci. U.S.A.* **116**, 5681–5686 (2019).
83. A. Berg, S. Patel, P. Aukrust, C. David, M. Gonca, E. S. Berg, I. Dalen, N. Langeland, Increased severity and mortality in adults co-infected with malaria and HIV in Maputo, Mozambique: A prospective cross-sectional study. *PLOS ONE* **9**, e88257 (2014).
84. F. de Chaumont, S. Dallongeville, N. Chenouard, N. Hervé, S. Pop, T. Provoost, V. Meas-Yedid, P. Pankajakshan, T. Lecomte, Y. Le Montagner, T. Lagache, A. Dufour, J.-C. Olivo-Marin, Icy: An open bioimage informatics platform for extended reproducible research. *Nat. Methods* **9**, 690–696 (2012).
85. C. J. Harbort, P. V. Soeiro-Pereira, H. von Bernuth, A. M. Kaindl, B. T. Costa-Carvalho, A. Condino-Neto, J. Reichenbach, J. Roesler, A. Zychlinsky, B. Amulic, Neutrophil oxidative burst activates ATM to regulate cytokine production and apoptosis. *Blood* **126**, 2842–2851 (2015).
86. R. E. Young, R. D. Thompson, K. Y. Larbi, M. La, C. E. Roberts, S. D. Shapiro, M. Perretti, S. Nourshargh, Neutrophil elastase (NE)-deficient mice demonstrate a nonredundant role for NE in neutrophil migration, generation of proinflammatory mediators, and phagocytosis in response to zymosan particles in vivo. *J. Immunol.* **172**, 4493–4502 (2004).
87. E. F. Kenny, B. Raupach, U. Abu Abed, V. Brinkmann, A. Zychlinsky, Dnase1-deficient mice spontaneously develop a systemic lupus erythematosus-like disease. *Eur. J. Immunol.* **49**, 590–599 (2019).
88. P. Li, M. Li, M. R. Lindberg, M. J. Kennett, N. Xiong, Y. Wang, PAD4 is essential for antibacterial innate immunity mediated by neutrophil extracellular traps. *J. Exp. Med.* **207**, 1853–1862 (2010).
89. M. Swamydas, Y. Luo, M. E. Dorf, M. S. Lionakis, Isolation of mouse neutrophils. *Curr. Protoc. Immunol.* **110**, 3.20.1–3.20.15 (2015).
90. V. Brinkmann, C. Goosmann, L. I. Kühn, A. Zychlinsky, Automatic quantification of in vitro NET formation. *Front. Immunol.* **3**, 413 (2012).
91. M. J. Losman, T. M. Fasy, K. E. Novick, M. Monestier, Monoclonal autoantibodies to subnucleosomes from a MRL/Mp(−)+/+ mouse. Oligoclonality of the antibody response and recognition of a determinant composed of histones H2A, H2B, and DNA. *J. Immunol.* **148**, 1561–1569 (1992).
92. S. Weis, A. R. Carlos, M. R. Moita, S. Singh, B. Blankenhaus, S. Cardoso, R. Larsen, S. Rebelo, S. Schäuble, L. Del Barrio, G. Mithieux, F. Rajas, S. Lindig, M. Bauer, M. P. Soares, Metabolic adaptation establishes disease tolerance to sepsis. *Cell* **169**, 1263–1275.e14 (2017).

93. B. Amulic, A. Salanti, T. Lavstsen, M. A. Nielsen, K. W. Deitsch, An upstream open reading frame controls translation of *var2csa*, a gene implicated in placental malaria. *PLOS Pathog.* **5**, e1000256 (2009).
94. V. Barrera, O. A. Skorokhod, D. Baci, G. Gremo, P. Arese, E. Schwarzer, Host fibrinogen stably bound to hemozoin rapidly activates monocytes via TLR-4 and CD11b/CD18-integrin: A new paradigm of hemozoin action. *Blood* **117**, 5674–5682 (2011).
95. P. Viriyavejakul, V. Khachonsaksumet, C. Punsawad, Liver changes in severe *Plasmodium falciparum* malaria: Histopathology, apoptosis and nuclear factor kappa B expression. *Malar. J.* **13**, 106 (2014).
96. S. Virreira Winter, A. Zychlinsky, The bacterial pigment pyocyanin inhibits the NLRP3 inflammasome through intracellular reactive oxygen and nitrogen species. *J. Biol. Chem.* **293**, 4893–4900 (2018).
97. I. Vancurova, V. Miskolci, D. Davidson, NF-kappa B activation in tumor necrosis factor alpha-stimulated neutrophils is mediated by protein kinase Cdelta. Correlation to nuclear Iκ Bα. *J. Biol. Chem.* **276**, 19746–19752 (2001).

Acknowledgments: We thank the patients, physicians, nurses, and other staff at the Albert Schweitzer Hospital and Maputo Central Hospital for their support and aid during our study. We also thank K. Seydel and T. Taylor for access to histopathology samples. **Funding**: B.A. is an MRC Career Development Fellow. A.J.C. was supported by MRC and the UK Department for International Development (DFID) under the MRC/DFID Concordat agreement and is also part of the EDCTP2 program supported by the European Union (MR/L006529/1 to A.J.C.). A.G. was supported by an Imperial College Dean's Internship Award. The Francis Crick Institute receives its core funding from the UK Medical Research Council (FC10101), Cancer Research UK (FC001101), and Wellcome (FC001101). J.L. is a Wellcome Senior Investigator (WT102907MA).
Author contributions: B.A., S.L.K., A.Z., A.J.C., C.A.M., and B.R. conceived and designed the experiments. S.L.K., B.A., F.A., and A.G. performed the experiments. U.A.-A., V.B., and A.G. performed microscopy. A.B., R.K., V.B., S.P.H., S.P., K.O., B.M., and C.A.M. contributed clinical samples. D.C., J.L., and E.S. contributed reagents/materials. B.A., S.L.K., and A.Z. wrote/drafted and finalized the paper. All authors read and approved the final manuscript. **Competing interests:** The authors declare that they have no competing interests. **Data and materials availability:** All data needed to evaluate the conclusions in the paper are present in the paper or the Supplementary Materials. The DNase 1 knockout mouse strain used in the study is available as frozen embryos from A.Z. (contact zychlinsky@mpiib-berlin.mpg.de).

Submitted 13 November 2018
Resubmitted 4 June 2019
Accepted 17 September 2019
Published 18 October 2019
10.1126/sciimmunol.aaw0336

Citation: S. L. Knackstedt, A. Georgiadou, F. Apel, U. Abu-Abed, C. A. Moxon, A. J. Cunnington, B. Raupach, D. Cunningham, J. Langhorne, R. Krüger, V. Barrera, S. P. Harding, A. Berg, S. Patel, K. Otterdal, B. Mordmüller, E. Schwarzer, V. Brinkmann, A. Zychlinsky, B. Amulic, Neutrophil extracellular traps drive inflammatory pathogenesis in malaria. *Sci. Immunol.* **4**, eaaw0336 (2019).

Science Immunology

Neutrophil extracellular traps drive inflammatory pathogenesis in malaria

Sebastian Lorenz Knackstedt, Athina Georgiadou, Falko Apel, Ulrike Abu-Abed, Christopher A. Moxon, Aubrey J. Cunnington, Bärbel Raupach, Deirdre Cunningham, Jean Langhorne, Renate Krüger, Valentina Barrera, Simon P. Harding, Aase Berg, Sam Patel, Kari Otterdal, Benjamin Mordmüller, Evelin Schwarzer, Volker Brinkmann, Arturo Zychlinsky and Borko Amulic

Sci. Immunol. **4**, eaaw0336.
DOI: 10.1126/sciimmunol.aaw0336

Neutrophil-derived NETs make malaria worse

The role of neutrophils in the inflammation and tissue pathology associated with malaria infection is poorly understood. Knackstedt *et al.* used samples from patients infected with the *Plasmodium falciparum* parasite, as well as a mouse model of malaria, to investigate the contributions of neutrophils and neutrophil extracellular traps (NETs) to disease pathogenesis. Heme released from parasitized red blood cells induced formation of intravascular NETs, leading to an increase in emergency granulopoiesis and an enhancement in the capacity of endothelial cells to bind infected erythrocytes. These findings demonstrate that neutrophil-derived NETs exacerbate malarial immunopathology, opening the door to targeting NETs as part of human malaria therapy.